Null geodesics in the metric of a line mass

Jacob van Peet
Marcel Haas
Sebastiaan Keek

13th July 2005

Abstract

We study the path of a photon as caused by a "cosmic string", a hypothetical mass distribution with zero radius. In order to do so we begin by equating the Ricci tensor to zero. Using variational calculus the Christoffel symbols are obtained. With those symbols we're able to solve the Ricci tensor components. In the end a solution for the metric is obtained containing two constants.

One of the constants is fixed by comparing the obtained metric to the Newtonian limit. Since one constant couldn't be solved we divert to the Weyl metric. Using that metric we calculate the photon orbits. We also do that with an extra metric that shows a conical spacetime. This cone shape is used as an explanation for distortion free deflection of light which happens in gravitational lensing.

Contents

1 Introduction

Two intensively studied fields in contemporary physics are the General Theory of Relativity (GR) and string theory. Whereas of course the latter is a promising attempt to combine GR with quantum mechanics, there recently appeared a second connection between both, see [1]. The importance of this second connection, which is in the area of macroscopic strings and the deformation of space-time they exhibit, for cosmology remains to be seen, but some interesting physics will not pass unnoticed.

1.1 Cosmic strings

String theory is meant to be a theory of everything, and therefore it should also explain the universe. String theory can give rise to inflation, see [5]. In this process a special kind of string is formed. These strings represent trapped energy. To lower this energy (as nature always tries) the strings will tend to shrink. The expansion of the universe, however, stretches them. These strings will be either extremely long, or closed loops. If there are strings longer than (or with a radius bigger than) the radius of the visible universe, they would still exist today.

The important thing about cosmic strings is their stability. The kind of strings that were able to survive until today should either be closed loops, or open strings, longer than the radius of the visible universe (well approximated by an infinite length). Because there is trapped potential energy in these objects, a mass per unit length can be assigned to them. In this case cosmic strings are a 'source of gravity'.

1.2 Two-dimensional gravity and cosmic strings

If we focus to the concept of the infinitely long string, the gravitational problem corresponding to this mass-distribution is that of 2-dimensional gravity, because of the translational symmetry along the length of the string. Actually it is of course better to call this gravity in $2+1$ dimensions, because the 2 only refers to the spatial dimensions.

From a theoretical point of view, this kind of gravity is already investigated in some detail. In this $2+1$ dimensional world some remarkable properties of the gravitational potential and space-time around masses will be adressed in this report.

1.3 Observations

The reason for this investigation is the fact that recently two possible discoveries of gravitational lensing by strings have been reported (see [6] and [7]). Both candidates can in principle be explained by other means, though a cosmic string seems a reasonable option. The lensing by cosmic strings (or lensing around a point mass in $2+1$ dimensions) has some remarkable properties, that will be explained in this report.

1.4 This report

This reported is structured as follows. First we derive the Newtonian limit for an infinite line mass. We need this limit in order to fix the constants when deriving a solution for the Einstein equations.

The deriving of the Einstein equations is the subject of the next section. After that we switch to the Weyl metric of a line mass. We solve the Weyl metric numerically and present the resulting photon orbits.

We do the same with another axisymmetric metric. We will show that spacetime of this metric has cone-like properties. Because of those properties, the flat space can produce double, distortion free, images.

In all derivations and calculations it is assumed that the cosmic string is perpendicular to the line connecting the observer and the observed object.

2 The Newtonian limit of a line mass

The Newtonian version of the gravitational field of an infinitely long and thin linemass along de z-axis in polar coordinates can be determined from the so called Newton field equation:

$$\nabla^2\Phi = 4\pi G\rho \tag{1}$$

In which Φ is the scalargravitational potential, G is the gravitational constant and ρ is the mass density (in this case a delta function at $r=0$). In such a potential, the gravitational force acting on a particle with mass m is given by

$$\mathbf{F}_G = -m\overrightarrow{\nabla}\Phi \tag{2}$$

2.1 The potential

With the help of the well known theorems for vector analysis, equation 1 can be written in integral form:

$$\oint_{\partial V} (\overrightarrow{\nabla}\Phi) \cdot \mathbf{da} = 4\pi G \int_V \rho \, \mathrm{d}\tau \tag{3}$$

for the potential in a volume V, with (closed) boundary ∂V. This form is equivalent to a Gauss-law in electrodynamics and we will therefore call it the gravitational Gauss law. We also can construct a gravitational Gaussian surface. We choose a cylinder with its axis along the z-axis. By (rotational) symmetrical arguments one can argue that on the mantle of this cylinder the potential is constant. The gradient of the potential will be point radially away from the axis, because of the translational symmetry along the z-axis. The top and bottom of our cylinder therefore have zero integrands.

The integral on the right can be seen as the enclosed mass (it is after all a volume integral over the density). We will call the mass per unit length μ. If our Gaussian cylinder has length l and radius r (so we can calculate the gradient of the potential at a distance r) equation 3 will become

$$2\pi r l \overrightarrow{\nabla}\Phi = 4\pi G \mu l \hat{\mathbf{r}} \tag{4}$$

which reduces to

$$\overrightarrow{\nabla}\Phi = \frac{2G\mu}{r}\hat{\mathbf{r}} \tag{5}$$

To get an implicit description of the potential we have to integrate this from the z-axis to a certain distance r:

$$\Phi = \int \overrightarrow{\nabla}\Phi \cdot \mathbf{dl} = 2G\mu \ln r \tag{6}$$

2.2 Newtonian approximation of the metric

With the help of the potential in equation 6, we can construct a newtonian approximation of the metric. Of course it is not possible to construct an exact metric that will give rise to the forces described by equation 2, because newtonian gravity is not a metric theory (it does not confirm with special relativity), but we can try to get as close as possible.

In order to do so we start by giving the classical equation of motion in a gravitational field:

$$\frac{\mathrm{d}^2 x^i}{\mathrm{d}t^2} + \frac{\partial \Phi}{\partial x^i} = 0 \tag{7}$$

In this equation of course, the i refers to the three spatial coordinates (r, φ, z), so the partial derivative only has a non-zero value for the r-component. The t mentioned herein is the universal absolute time. We can parametrize the four dimensions used in general relativity by parametrizing with the proper time λ; a curve is described by the functions $(t(\lambda), r(\lambda), \varphi(\lambda), z(\lambda))$. Because we are in a classical, Euclidean universe, this proper time can only relate to the universal time as $\lambda = at + b$, so the second derivative in the equation of motion (equation 7) will become zero when evaluating it for the time-component of the coordinates. With this parametrization, equation 7 can be written as

$$\frac{\mathrm{d}^2 t}{\mathrm{d}\lambda^2} = 0 \quad , \quad \frac{\mathrm{d}^2 x^i}{\mathrm{d}\lambda^2} + \frac{\partial \Phi}{\partial x^i}\left(\frac{\mathrm{d}t}{\mathrm{d}\lambda}\right)^2 = 0 \tag{8}$$

Comparing this to the well known geodesic equation, we can easily recognize the Christoffel symbols. The only non-zero components are

$$\Gamma^i_{tt} = \frac{\partial \Phi}{\partial x^i} \tag{9}$$

In which $i = r, \varphi, z$. Because the potential only depends on the r-coordinate the only Christoffel symbol that is non-zero is $\Gamma^r_{tt} = \frac{2G\mu}{r}$. This also leaves us with only 1 non-zero component in the Riemann-tensor:

$$R^i_{tjt} = \frac{\partial^2 \Phi}{\partial x^i \partial x^j} \quad \rightarrow \quad R^r_{trt} = \frac{\partial^2 \Phi}{\partial r^2} = -\frac{2G\mu}{r^2} \tag{10}$$

As stated before, newtonian gravity is not a metric theory. Therefore we cannot find a metric which generates the Christoffel symbols in equation 9 exactly. We weren't able to obtain an approximating metric. However, equation 6 is useful in fixing one of the constants in the metric (see section 3.4).

3 Solution of the Einstein equations

The Einstein equations are given by

$$G^{\mu\nu} = -\frac{8\pi G}{c^2} T^{\mu\nu} \tag{11}$$

where $G^{\mu\nu}$ is the Einstein field tensor and $T^{\mu\nu}$ contains all information about the energy and mass distribution. Since we're only interested in solving the Einstein equations in empty space it follows that $T^{\mu\nu} = 0$ and therefore that $G^{\mu\nu} = R^{\mu\nu} - \frac{1}{2} g^{\mu\nu} R = 0$. It can be shown that it is sufficient to solve for

$$R_{\mu\nu} = 0 \tag{12}$$

3.1 Using the symmetries

We are seeking the solution of a cylindrical symmetric and static mass distribution (a line mass) so we choose cylindrical coordinates (t, r, φ, z) in which t stands for the time coordinate, r for the radial coordinate and φ for the angular coordinate around de z-axis.

Since the solution will be cylindrical symmetric, the metric will not depend on on cross terms like $g_{r\varphi}drd\varphi$. It follows that all terms like $g_{r\varphi}$ and $g_{t\varphi}$ are zero since the length of a curve in the positive φ direction should not be different from the length of a curve in the negative direction. The same reasoning brings us to the conclusion that only the terms g_{tt}, g_{rr}, $g_{\varphi\varphi}$ and g_{zz} are not 0.

Since we're dealing with cylindrical symmetry, all angular information of the metric is contained within the $d\varphi^2$ term. Furthermore, since we're looking at static solutions all $g_{\alpha\beta}$ terms should be independent of time.

The most general line element is in terms of coordinates (t', r', φ, z)

with G Newton's gravitational constant, μ the mass per unit length and r the radial coordinate. Since it's known that in the weak field limit the g_{tt} term is given by

$$g_{tt} = -\left(1 + \frac{2\Phi_{grav}}{c^2}\right)$$

the g_{tt} term for the line mass becomes

$$g_{tt} = -\left(1 + \frac{4G\mu}{c^2}\ln r\right) \tag{14}$$

The function $\mathrm{e}^{2\Phi(r)}$ (remark that $\Phi(r) \neq \Phi_{grav}(r)$) should have the same limit, so it follows

$$\lim_{r\to\infty} \Phi\left(r\right) = \frac{1}{2}\ln\left(1 + \frac{4G\mu}{c^2}\ln r\right) \tag{15}$$

Unfortunately we were not able to obtain the full Newtonian expression for an infinite line mass. Therefore we didn't obtain an expression for the limit of $\Lambda(r)$.

Finally we have arrived at an expression for the line element that will serve as a starting point for solving the Christoffel symbols

$$\mathrm{d}s^2 = -\mathrm{e}^{2\Phi(r)}\mathrm{d}t^2 + \mathrm{e}^{2\Lambda(r)}\mathrm{d}r^2 + r^2\mathrm{d}\varphi^2 + \mathrm{d}z^2 \tag{16}$$

3.2 Christoffel symbols

Equation 16 gives us L

$$L = -\mathrm{e}^{2\Phi(r)}\dot{t}^2 + \mathrm{e}^{2\Lambda(r)}\dot{r}^2 + r^2\dot{\varphi}^2 + \dot{z}^2 \tag{17}$$

by solving the Euler-Lagrange equations

$$\frac{\mathrm{d}}{\mathrm{d}\lambda}\frac{\partial L}{\partial \dot{x}^\alpha} - \frac{\partial L}{\partial x^\alpha} = 0$$

and comparing them to the geodesic equation

$$\ddot{x}^\alpha + \Gamma^\alpha_{\beta\gamma}\dot{x}^\beta\dot{x}^\gamma = 0$$

we can obtain the Christoffel symbols $\Gamma^\alpha_{\beta\gamma} = \Gamma^\alpha_{\gamma\beta}$. For the rest of this chapter the following notation is used

$$\begin{aligned}\Phi' &\equiv \frac{\mathrm{d}\Phi\left(r\right)}{\mathrm{d}r}\\ \dot{\Phi} &\equiv \frac{\mathrm{d}\Phi\left(r\right)}{\mathrm{d}\lambda}\end{aligned}$$

3.2.1 t component

The Euler Lagrange equations for the t component are solved

$$\frac{\mathrm{d}}{\mathrm{d}\lambda}\frac{\partial L}{\partial \dot{t}} - \frac{\partial L}{\partial t} = 0 \Rightarrow \frac{\mathrm{d}}{\mathrm{d}\lambda}\frac{\partial L}{\partial \dot{t}} = 0$$

$$\frac{\mathrm{d}}{\mathrm{d}\lambda}\left(-2\mathrm{e}^{2\Phi}\dot{t}\right) = -2\mathrm{e}^{2\Phi}\ddot{t} - 4\mathrm{e}^{2\Phi}\Phi'\dot{r}\dot{t} = 0$$

$$\Rightarrow \ddot{t} + 2\Phi'\dot{r}\dot{t} = 0$$

Therefore we conclude

$$\Gamma^t_{rt} = \Gamma^t_{tr} = \Phi' \tag{18}$$

All other $\Gamma^t_{\alpha\beta}$ are 0.

3.2.2 r component

The Euler Lagrange equations for the r component are solved

$$\frac{\mathrm{d}}{\mathrm{d}\lambda}\frac{\partial L}{\partial \dot{r}} - \frac{\partial L}{\partial r} = 0 \Rightarrow \frac{\mathrm{d}}{\mathrm{d}\lambda}\left(2\mathrm{e}^{2\Lambda}\dot{r}\right) - \left(-2\mathrm{e}^{2\Phi}\Phi'\dot{t}^2 + 2\mathrm{e}^{2\Lambda}\Lambda'\dot{r}^2 + 2r\dot{\varphi}^2\right) = 0$$

$$\Rightarrow 2\mathrm{e}^{2\Lambda}\ddot{r} + 4\mathrm{e}^{2\Lambda}\Lambda'\dot{r}^2 + 2\mathrm{e}^{2\Phi}\Phi'\dot{t}^2 - 2\mathrm{e}^{2\Lambda}\Lambda'\dot{r}^2 - 2r\dot{\varphi}^2 = 0$$

$$\Rightarrow \ddot{r} + \Lambda'\dot{r}^2 + \mathrm{e}^{2\Phi-2\Lambda}\Phi'\dot{t}^2 - r\mathrm{e}^{-2\Lambda}\dot{\varphi}^2 = 0$$

Therefore we conclude

$$\begin{aligned} \Gamma^r_{rr} &= \Lambda' \\ \Gamma^r_{tt} &= \mathrm{e}^{2\Phi-2\Lambda}\Phi' \\ \Gamma^r_{\varphi\varphi} &= -r\mathrm{e}^{-2\Lambda} \end{aligned} \tag{19}$$

All other $\Gamma^r_{\alpha\beta}$ are 0.

3.2.3 φ component

The Euler Lagrange equations for the φ component are solved

$$\frac{\mathrm{d}}{\mathrm{d}\lambda}\frac{\partial L}{\partial \dot{\varphi}} - \frac{\partial L}{\partial \varphi} = 0 \Rightarrow \frac{\mathrm{d}}{\mathrm{d}\lambda}\left(2r^2\dot{\varphi}\right) = 0$$

$$\Rightarrow 4r\dot{r}\dot{\varphi} + 2r^2\ddot{\varphi} = 0 \Rightarrow \ddot{\varphi} + 2\frac{1}{r}\dot{r}\dot{\varphi} = 0$$

Therefore we conclude

$$\Gamma^\varphi_{r\varphi} = \Gamma^\varphi_{\varphi r} = \frac{1}{r} \tag{20}$$

All other $\Gamma^\varphi_{\alpha\beta}$ are 0.

3.2.4 z component

The Euler Lagrange equations for the z component are solved

$$\frac{\mathrm{d}}{\mathrm{d}\lambda}\frac{\partial L}{\partial \dot{z}} - \frac{\partial L}{\partial z} = 0 \Rightarrow \frac{\mathrm{d}}{\mathrm{d}\lambda}\left(2\dot{z}\right) = 0 \Rightarrow 2\ddot{z} = 0 \Rightarrow \ddot{z} = 0$$

Therefore we conclude that all $\Gamma^z_{\alpha\beta}$ are 0.

3.3 Ricci tensor

The Ricci tensor is given by

$$\begin{aligned} R_{\mu\nu} &= \Gamma^\alpha_{\mu\alpha,\nu} - \Gamma^\alpha_{\mu\nu,\alpha} - \Gamma^\alpha_{\mu\nu}\Gamma^\beta_{\alpha\beta} + \Gamma^\alpha_{\mu\beta}\Gamma^\beta_{\nu\alpha} \\ &= \tfrac{\partial}{\partial x^\nu}\left(\Gamma^\alpha_{\mu\alpha}\right) - \tfrac{\partial}{\partial x^\alpha}\left(\Gamma^\alpha_{\mu\nu}\right) - \Gamma^\alpha_{\mu\nu}\Gamma^\beta_{\alpha\beta} + \Gamma^\alpha_{\mu\beta}\Gamma^\beta_{\nu\alpha} \end{aligned} \tag{21}$$

3.3.1 tt component

Combining equations 12 and 21 we find that $R_{tt} = 0$ or

$$R_{tt} = -\frac{\partial}{\partial r}\left(\Gamma^r_{tt}\right) - \Gamma^r_{tt}\left(\Gamma^t_{rt} + \Gamma^r_{rr} + \Gamma^\varphi_{r\varphi} + \Gamma^z_{rz}\right) + 2\Gamma^r_{tt}\Gamma^t_{tr} = 0$$

Insert the Christoffel symbols from section 3.2

$$\begin{aligned} R_{tt} = 0 &= -\tfrac{\partial}{\partial r}\left(\mathrm{e}^{2\Phi-2\Lambda}\Phi'\right) - \mathrm{e}^{2\Phi-2\Lambda}\Phi'\left(\Phi' + \Lambda' + \tfrac{1}{r}\right) + 2\mathrm{e}^{2\Phi-2\Lambda}\Phi'\Phi' \\ &= -\left(2\Phi' - 2\Lambda'\right)\mathrm{e}^{2\Phi-2\Lambda}\Phi' - \mathrm{e}^{2\Phi-2\Lambda}\Phi'' \\ &\quad -\mathrm{e}^{2\Phi-2\Lambda}\Phi'\left(\Phi' + \Lambda' + \tfrac{1}{r}\right) + 2\mathrm{e}^{2\Phi-2\Lambda}\Phi'^2 \\ &= -\left(2\Phi' - 2\Lambda'\right)\Phi' - \Phi'' - \Phi'\left(\Phi' + \Lambda' + \tfrac{1}{r}\right) + 2\Phi'^2 \end{aligned}$$

From this last expression a differential equation for Φ and Λ is found

$$\Phi'' + \frac{1}{r}\Phi' - \Phi'\Lambda' + \Phi'^2 = 0 \tag{22}$$

3.3.2 rr component

Combining equations 12 and 21 we find that $R_{rr} = 0$ or

$$\begin{aligned} R_{rr} &= \tfrac{\partial}{\partial r}\left(\Gamma^t_{rt} + \Gamma^r_{rr} + \Gamma^\varphi_{r\varphi}\right) - \tfrac{\partial}{\partial r}\left(\Gamma^r_{rr}\right) \\ &\quad -\Gamma^r_{rr}\left(\Gamma^t_{rt} + \Gamma^r_{rr} + \Gamma^\varphi_{r\varphi}\right) + \Gamma^t_{rt}\Gamma^t_{rt} \\ &\quad +\Gamma^r_{rr}\Gamma^r_{rr} + \Gamma^\varphi_{r\varphi}\Gamma^\varphi_{r\varphi} = 0 \end{aligned}$$

Insert the Christoffel symbols from section 3.2

$$\begin{aligned} R_{rr} = 0 &= \tfrac{\partial}{\partial r}\left(\Phi' + \tfrac{1}{r}\right) - \Lambda'\left(\Phi' + \Lambda' + \tfrac{1}{r}\right) + \Phi'^2 + \Lambda'^2 + \tfrac{1}{r^2} \\ &= \Phi'' - \tfrac{1}{r^2} - \Lambda'\Phi' - \Lambda'^2 - \tfrac{1}{r}\Lambda' + \Phi'^2 + \Lambda'^2 + \tfrac{1}{r^2} \end{aligned}$$

From this last expression another differential equation for Φ and Λ is found

and it follows that

$$\begin{aligned} \mathrm{e}^{2\Phi(r)} &= 1 + \frac{4G\mu}{c^2}\ln r \\ \mathrm{e}^{2\Lambda(r)} &= \mathrm{e}^{2\cdot constant - \ln\left(1+\frac{4G\mu}{c^2}\ln r\right)} = \mathrm{e}^{2\cdot constant}\mathrm{e}^{-\ln\left(1+\frac{4G\mu}{c^2}\ln r\right)} \\ &= \frac{K_1}{1+\frac{4G\mu}{c^2}\ln r} \end{aligned} \tag{32}$$

with $K_1 > 0$.

Insert equations 32 into equation 16 and the line element for a static cylindrical symmetric mass distribution becomes

$$\mathrm{d}s^2 = -\left(1 + \frac{4G\mu}{c^2}\ln r\right)\mathrm{d}t^2 + \frac{K_1}{1+\frac{4G\mu}{c^2}\ln r}\mathrm{d}r^2 + r^2\mathrm{d}\varphi^2 + \mathrm{d}z^2 \tag{33}$$

4 Analytical solutions to the Weyl metric

One of the "classical" tests of general relativity is the deflection of light. The deflection of light for an infinite line mass is the subject for the following sections.

Since our metric (33) still contains an undetermined constant, we first try an alternative metric i.e. the Weyl metric. We will see that it yields no analytical solution, so we switch to the Newtonian approximation but will also see that it yields no analytical solution.

In the next section we will give the numerical results of the Weyl metric and a graphical representation of those results.

4.1 The Weyl metric

We have the Weyl metric

$$\mathrm{d}s^2 = -r^{4m}\mathrm{d}t^2 + r^{-4m+8m^2}\mathrm{d}r^2 + r^{2-4m}\mathrm{d}\varphi^2 \tag{34}$$

so the Euler-LaGrange equations become

$$L = -r^{4m}\dot{t}^2 + r^{-4m+8m^2}\dot{r}^2 + r^{2-4m}\dot{\varphi}^2 \tag{35}$$

and for the t and φ components we have

$$\frac{\mathrm{d}}{\mathrm{d}\lambda}\left(\frac{\partial L}{\partial \dot{x}^\alpha}\right) - \frac{\partial L}{\partial x^\alpha} = 0 \Rightarrow \frac{\mathrm{d}}{\mathrm{d}\lambda}\left(\frac{\partial L}{\partial \dot{x}^\alpha}\right) = 0 \Rightarrow \frac{\partial L}{\partial \dot{x}^\alpha} = constant \tag{36}$$

For the **t component** (the conjugate momentum to the t coordinate is the energy)

$$-2r^{4m}\dot{t} = K_1 \Rightarrow \dot{t} = \frac{-K_1}{2r^{4m}} \tag{37}$$

and for the φ **component** (the conjugate momentum to the φ coordinate is the angular momentum)

$$2\dot{\varphi}r^{2-4m} = K_2 \Rightarrow \dot{\varphi} = \frac{K_2}{2r^{2-4m}} \tag{38}$$

Insert 37 and 38 back into 34 and use the fact that $ds^2 = 0$ for photons

$$\frac{-K_1^2}{4r^{4m}} + r^{-4m+8m^2}\dot{r}^2 + \frac{K_2^2}{4r^{2-4m}} = 0 \tag{39}$$

The approach to solve 39 following the lecture notes does not seem to yield an analytical solution:

Take equation 39 and multiply by $4r^{4m}$

$$-K_1^2 + 4r^{8m^2}\dot{r}^2 + \frac{K_2^2}{r^{2-8m}} = 0 \tag{40}$$

Now take the derivative

$$\begin{aligned} 32m^2 r^{8m^2-1}\dot{r}\dot{r}^2 + 8r^{8m^2}\dot{r}\ddot{r} - (2-8m)\frac{K_2^2}{r^{3-8m}}\dot{r} &= 0 \\ \ddot{r} + 4m^2\frac{1}{r}\dot{r}^2 - \frac{1}{8}(2-8m)\frac{K_2^2}{r^{3-8m-8m^2}} &= 0 \end{aligned} \tag{41}$$

Now use

$$u = \frac{1}{r} \tag{42}$$

$$u' \equiv \frac{\mathrm{d}u}{\mathrm{d}\varphi} = \frac{\dot{u}}{\dot{\varphi}} = \frac{-\frac{1}{r^2}\dot{r}}{\frac{K_2}{2r^{2-4m}}} = -\frac{2}{K_2 r^{4m}}\dot{r} \tag{43}$$

$$u'' \equiv \frac{\mathrm{d}^2u}{\mathrm{d}\varphi^2} = \frac{\mathrm{d}u'}{\mathrm{d}\varphi} = \frac{\frac{\mathrm{d}u'}{\mathrm{d}\lambda}}{\frac{\mathrm{d}\lambda}{\mathrm{d}\varphi}} = \frac{\frac{8m}{K_2 r^{4m+1}}\dot{r}^2 - \frac{2}{K_2 r^{4m}}\ddot{r}}{\frac{K_2}{2r^{2-4m}}} \tag{44}$$

$$= \frac{16m}{K_2^2}r^{1-8m}\dot{r}^2 - \frac{4}{K_2^2}r^{2-8m}\ddot{r} \tag{45}$$

Substituting these expressions for u, u' and u'' into 41 yields a useful expression in the lecture notes for the Schwarzschild metric, but in this case of the line mass it doesn't.

4.2 The Weyl metric in the Newtonian limit

Since we weren't able to obtain an analytical solution to the Weyl metric, we try a simplification. We have (lecture notes [3] equation 12.9) the following Newtonian limit for the Weyl metric

$$\mathrm{d}s^2 = -(1+4m\ln r)\mathrm{d}t^2 + (1-4m\ln r)(\mathrm{d}r^2 + r^2\mathrm{d}\varphi^2) \tag{46}$$

So

$$L = -(1+4m\ln r)\dot{t}^2 + (1-4m\ln r)\dot{r}^2 + (1-4m\ln r)r^2\dot{\varphi}^2 \tag{47}$$

and for the t and φ components we again have

$$\frac{\mathrm{d}}{\mathrm{d}\lambda}\left(\frac{\partial L}{\partial \dot{x}^\alpha}\right) - \frac{\partial L}{\partial x^\alpha} = 0 \Rightarrow \frac{\mathrm{d}}{\mathrm{d}\lambda}\left(\frac{\partial L}{\partial \dot{x}^\alpha}\right) = 0 \Rightarrow \frac{\partial L}{\partial \dot{x}^\alpha} = constant \tag{48}$$

For the **t component**

$$-2(1+4m\ln r)\dot{t} = K_1 \Rightarrow \dot{t} = \frac{-K_1}{2(1+4m\ln r)} \tag{49}$$

and for the φ **component**

$$2(1-4m\ln r)r^2\dot{\varphi} = K_2 \Rightarrow \dot{\varphi} = \frac{K_2}{2(1-4m\ln r)r^2} \tag{50}$$

Insert 49 and 50 back into 46

$$\frac{-K_1^2}{4(1+4m\ln r)} + (1-4m\ln r)\dot{r}^2 + \frac{K_2^2}{4(1-4m\ln r)r^2} \tag{51}$$

Again this doesn't lead to an expression usable for determining analytically the deflection angle of light. Perhaps other substitutions (like the $u = 1/r$ from the lecture notes) could work, but we weren't able to obtain them.

5 Numerical solutions to the Weyl metric

5.1 Introduction

In this section we return to equation 34 and take a look at the behavior of light in the space this metric describes. We start by generating a general method (section 5.2) that reshapes any metric into an equation for the effective potential and the full equations for the motion of photons. Calculating

5.2 General Method

We start our derivation of a general method for obtaining photon orbits by introducing the standard metric in polar coordinates

$$\mathrm{d}s^2 = f(r)\mathrm{d}t^2 + g(r)\mathrm{d}r^2 + h(r)\mathrm{d}\phi^2 \tag{52}$$

This is the general metric in polar-coordinates and applies to both the Schwarzschild metric and the Weyl metric. This is convenient as it allows us to create a general method to work with and test against known results. Keep in mind that the non-trivial term $\mathrm{d}z^2$ is omitted from the general calculations to keep things simple. It should pose no problem to repeat the following series of calculations should we be interested in the effect of this constant of motion.

We want to solve equation 52 by using variational principles. Therefore we introduce

$$L = f(r)\dot{t}^2 + g(r)\dot{r}^2 + h(r)\dot{\phi}^2 \tag{53}$$

The Euler-Lagrange equations are then given by equation 53. The corresponding constants of motion are given by

$$\frac{\partial L}{\partial \dot{t}} = -2f(r)\dot{t} = -2C_t \tag{54}$$

$$\frac{\partial L}{\partial \dot{\phi}} = 2h(r)\dot{\phi} = 2C_\phi \tag{55}$$

Plugging these back into equation 52 gives us:

$$\mathrm{d}s^2 = \frac{C_t^2}{f(r)} + g(r)\dot{r}^2 + \frac{C_\phi^2}{h(r)} \tag{56}$$

We further simplify equation 56 by isolating the constant related to $\mathrm{d}t^2$ (i.e. C_t) from the radial variable by multiplying the whole equation by $f(r)$

$$f(r)\mathrm{d}s^2 = C_t^2 + f(r)g(r)\dot{r}^2 + \frac{f(r)}{h(r)}C_\phi^2 \tag{57}$$

From here we can go two directions: finding an expression for the effective potential or obtaining the full equations of motion.

5.2.1 Effective potential

The effective potential allows us to to obtain some insight into orbits without explicitly solving equation 57 and thus predict any results we may obtain later by solving the full equations of motion.

Finding an equation for this effective potential starts by seeing that the constant C_t is related to the energy as in equation 58.

$$\frac{\partial L}{\partial \dot{t}} = -2f(r)\dot{t} = -2C_t = -2\sqrt{2\epsilon + 1} \tag{58}$$

Whereas the constant C_ϕ is related to the angular momentum as in equation 59.

$$\frac{\partial L}{\partial \dot{\phi}} = 2h(r)\dot{\phi} = 2C_\phi = 2l \tag{59}$$

Plugging this into equation 57 yields

$$f(r)\mathrm{d}s^2 = 2\epsilon + 1 + f(r)g(r)\dot{r}^2 + \frac{f(r)}{h(r)}l^2 \tag{60}$$

Which can be rewritten to an expression for the energy term ϵ.

$$\epsilon = \frac{\mathrm{d}s^2}{2}f(r) - \frac{1}{2} - \frac{l^2 f(r)}{2h(r)} - \frac{\dot{r}^2}{2}f(r)g(r) \tag{61}$$

We define the effective potential as

$$V_{eff} = \frac{\mathrm{d}s^2}{2}f(r) - \frac{1}{2} - \frac{l^2 f(r)}{2h(r)} \tag{62}$$

In equation 62 $\mathrm{d}s^2$ is determined by the object of interest. For photons we know that $\mathrm{d}s^2 = 0$ whereas for objects with mass $\mathrm{d}s^2 < 0$.

5.2.2 Equations of motion

If we now return to equation 57 and plug in $\mathrm{d}s^2 = 0$ for photons trajectories, and differentiate the whole equation we are left with the following differential equation

$$0 = \dot{r}\left[f(\dot{r})\left\{\frac{C_\phi^2}{h(r)} + g(r)\dot{r}^2\right\} + f(r)\left\{g(\dot{r})\dot{r}^2 + 2g(r)\ddot{r} - \frac{l^2 h(\dot{r})}{h(r)^2}\right\}\right] \tag{63}$$

This equation gives us a value for $\ddot{r}$ as function of $\dot{r}$,r and the constant C_ϕ which may be included in the functions $f(r)$,$g(r)$ and $h(r)$. Using equation 63 and the appropriate boundary values for $r(0)$ and $\dot{r}(0)$ we can compute the full solution for r. Plugging this solution for r back into the equations 54 and 55 provides us with equations for $\dot{\phi}$ and $\dot{t}$. Those equations and the appropriate boundary values for $\phi(0)$ and $t(0)$ allow us to compute a complete path in all three coordinates r,ϕ and t.

5.3 Testing the general method with the Schwarzschild metric

We now have a general method that gives us, for a given metric in the shape of equation 52, the effective potential of particles and the full motion of light in the space described by this metric. We now apply this method on the Schwarzschild metric to verify the results our method produces. This would give us an indication if our method is correct, both mathematically and numerically, making sure any features of the spacetime are probably real and not some numerical artifact.

5.3.1 Effective potential

The Schwarzschild metric is given by:

$$\mathrm{d}s^2 = -(1 - \frac{2m}{r})\mathrm{d}t^2 + \frac{\mathrm{d}r^2}{1 - \frac{2m}{r}} + r^2(\sin\theta^2\mathrm{d}\phi^2 + \mathrm{d}\theta^2) \tag{64}$$

Taking $\theta = \frac{\pi}{2}$ and plugging this equation into equation 62 gives us:

$$V_{eff} = \frac{l^2}{2r^2} - \frac{ml^2}{r^3} - \frac{m}{r} \tag{65}$$

If we plot this equation in figure 1 observe familiar features such as a peak with increasing height as the angular momentum increases and the steep drop to $V_{eff} \to -\infty$ when $r \to 0$

5.3.2 Equations of motion

Inserting the Schwarzschild metric into equations 65, 58 and 59 yields the equations of motion for photons

$$\ddot{r} = \frac{l^2}{r^3} - \frac{3l^2m}{r^4} \tag{66}$$

$$\dot{\phi} = \frac{l}{r^2} \tag{67}$$

$$\dot{t} = \frac{1 - \frac{2m}{r}}{1} \tag{68}$$

Where the constant C_t was chosen to obtain $\dot{t} = 1$ in the absence of mass. By simply computing t and r for photons with starting values $\dot{r} = 1$ and $\dot{r} = -1$ we can produce light-cones in the space described by our metric. The result displayed in figure 2 shows the familiar features of Schwarzschild

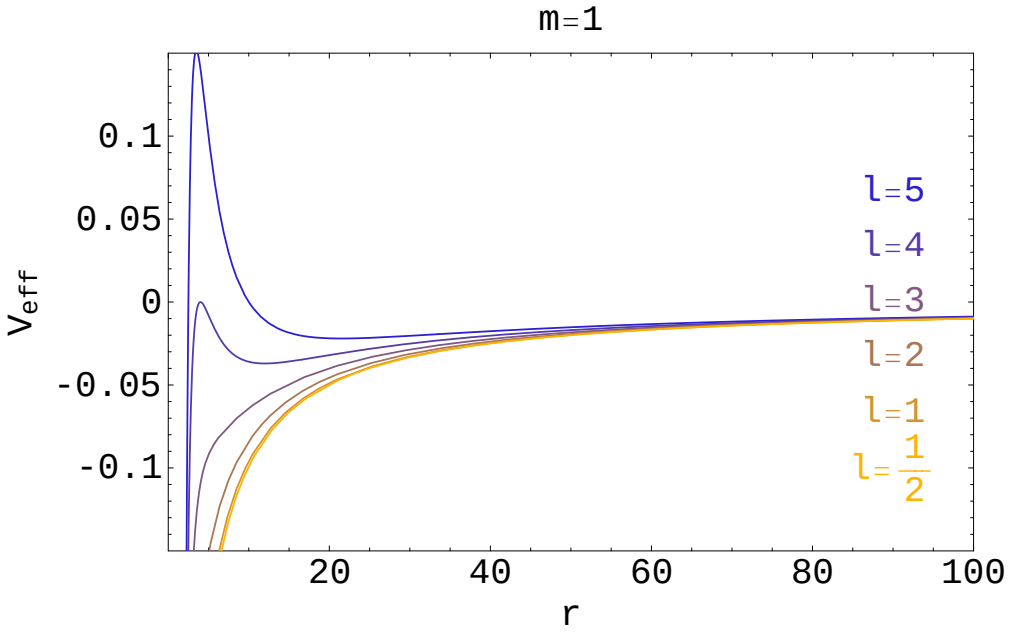

Figure 1: The standard Schwarzschild potential: $V_{eff} = \frac{l^2}{2r^2} - \frac{ml^2}{r^3} - \frac{m}{r}$ for the momenta: $l = 5, 4, 3.7, 3.464, 3, 1$

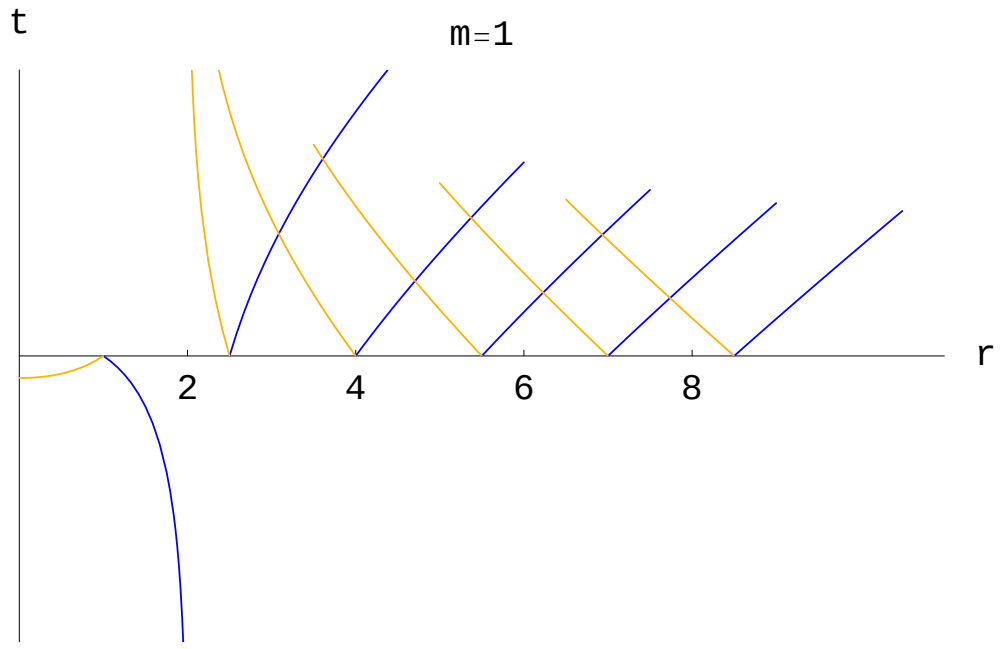

Figure 2: Light Cones plotting t as function of r with starting values $\dot{r} = 1$ (blue) and $\dot{r} = -1$ (orange).

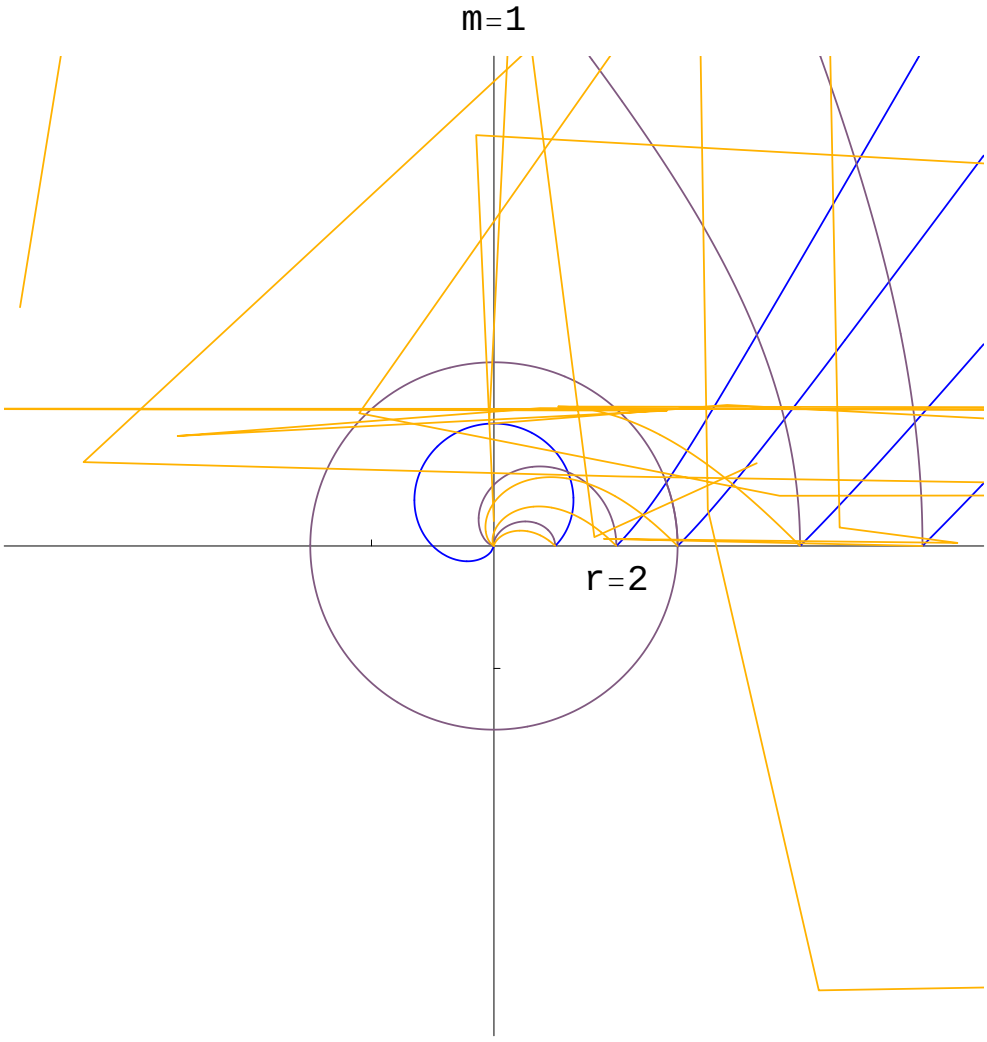

Figure 3: Graphical representation of photon paths combining r and ϕ using the starting directions $\dot{r} = 0$, $\dot{\phi} = \frac{1}{r}$ (grey); $\dot{r} = \sin\frac{\pi}{4}$, $\dot{\phi} = \frac{\sin\frac{\pi}{4}}{r}$ (blue) and $\dot{r} = -\sin\frac{\pi}{4}$, $\dot{\phi} = \frac{\sin\frac{\pi}{4}}{r}$ (orange).

space, for example the cones closer to the Schwarzschild radius are narrower. Computing both r and ϕ however gives us the full motion paths of photons and how those paths are influenced by mass. The results can be seen in figure 3. Here orange represents the starting values $\dot{r} = -\sin\frac{\pi}{4}$, $\dot{\phi} = \frac{\sin\frac{\pi}{4}}{r}$, gray represents $\dot{r} = 0$, $\dot{\phi} = \frac{1}{r}$ and blue $\dot{r} = \sin\frac{\pi}{4}$, $\dot{\phi} = \frac{\sin\frac{\pi}{4}}{r}$. The figure again shows us all the well known aspects. Including the stable orbit at $r = 3m$, all paths leading to $r = 0$ when emitted from $r = m$ and the bending of light.

5.3.3 The deflection of light

We conclude our tests with the most well known, and experimentally tested, feature of Schwarzschild gravity, the deflection of light. While figure 3 shows perfectly how light behaves near matter it is the end result which is most important to the distant observer. The process can be best described by figure 4 where a light beam originating from the lower left side of the figures, passes the point-mass and is deflected into the upper left part of the figures. Because this situation is symmetric around the x-axis we only need to simulate the orange part of the beam. This allows us to find a clear relation between the minimal distance of the photon to the point-mass and the angle between the incoming and outgoing trajectory. The results are plotted in figure 5 which shows us the deflection of light by calculating ϕ for $r \to \infty$ and $\dot{\phi} \to 0$. This deflection angle is plotted against r_{min} which is the starting r for an angular photon. Through this data a curve is fitted with $\phi = \frac{C}{r_{min}}$ where the constant C matches $4m$ which corresponds to the known relation known for deflection of light $\Delta = \frac{4m}{r_{min}}$.

5.4 Using the Weyl metric

Since the general method yields the expected answers for the Schwarzschild metric we continue to do the same for the Weyl metric.

$$L = -r^{4m}\dot{t}^2 + r^{-4m+8m^2}\dot{r}^2 + r^{2-4m}\dot{\phi}^2 \tag{69}$$

$$\frac{\partial L}{\partial \dot{t}} = -2r^{4m}\dot{t} = -2\sqrt{2\epsilon + 1} \tag{70}$$

$$\frac{\partial L}{\partial \dot{\phi}} = 2r^{2-4m}\dot{\phi} = 2l \tag{71}$$

From equation 71 we notice both $m = \frac{1}{4}$ and $m = \frac{1}{2}$ must be a special cases. For $m = \frac{1}{4}$ it follows that $r\dot{\phi}$ which is the physical radial velocity becomes constant whereas for $m = \frac{1}{2}$ the expression is independent of r and $\dot{\phi}$ becomes constant.

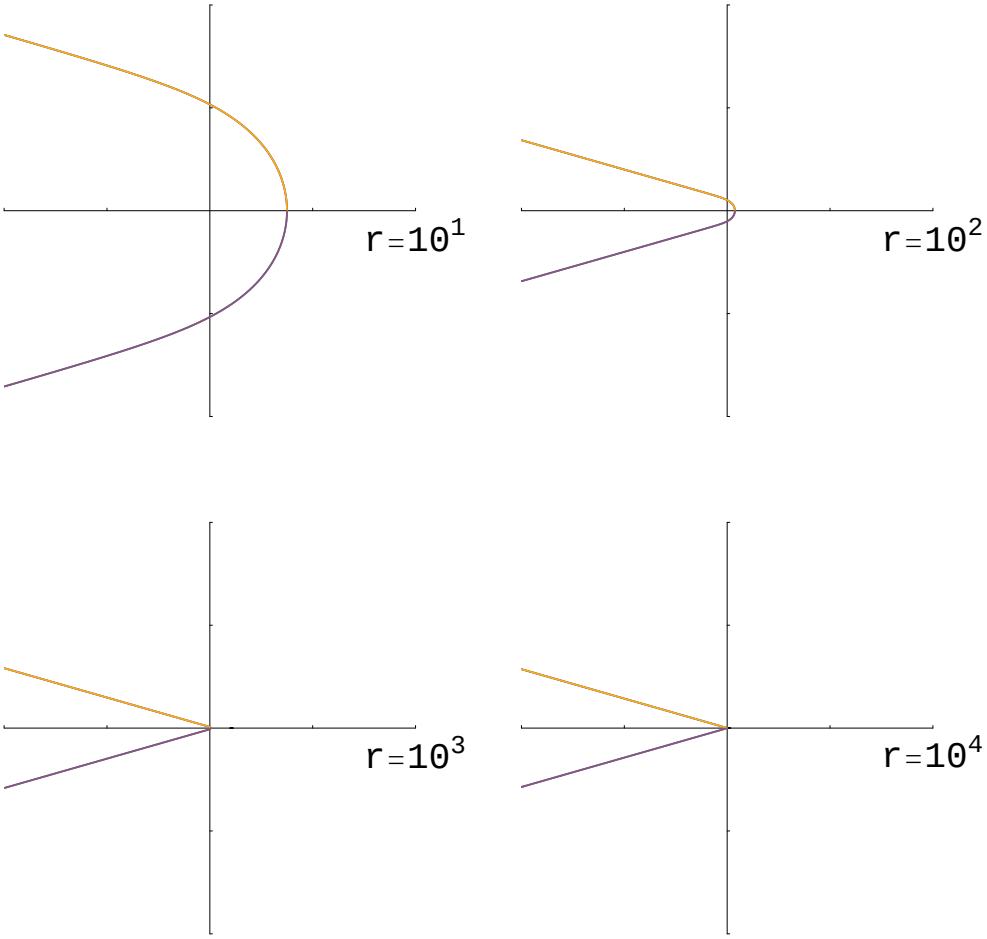

Figure 4: The path of a single photon passing $r = 3m$ at $\dot{r} = 0$ at several plot intervals.

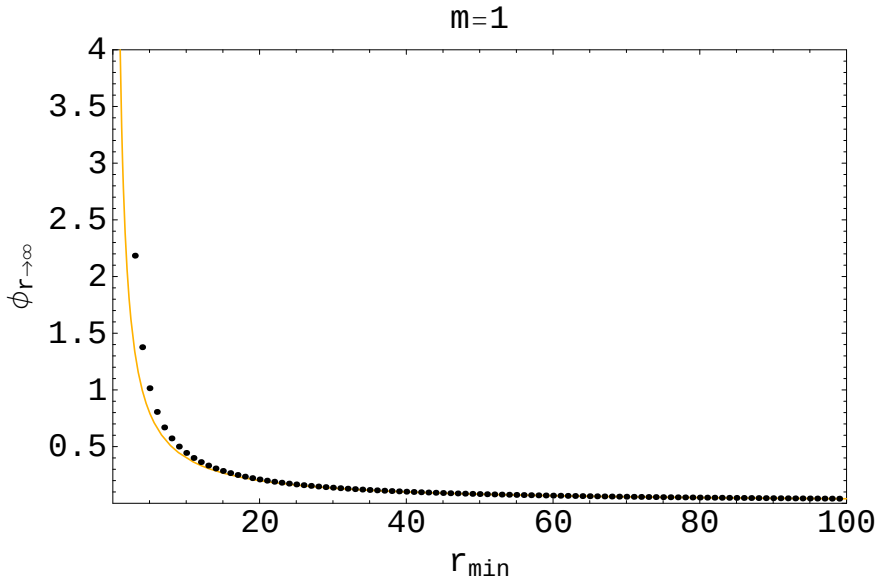

Figure 5: The deflection angle $2\phi_{r\to\infty}$ plotted against the minimal distance to the mass r_{min}. Dots: Numerical calculations, Curve: Fit to the data with $2\phi_{r\to\infty} = \frac{a}{r_{min}}$ where $a = 4m$

Plugging equations 70 and 71 back into equation 69 brings us again to the metric equation depending only on r, $\dot{r}$ and some constants.

$$L = -(1+2\epsilon)r^{-4m} + l^2 r^{4m-2} + r^{8m^2-4m}\dot{r}^2 \tag{72}$$

We reshape this equation and find the energy and the corresponding effective potential of photons. Here we limit ourselves to photons to use the equation as a tool to predict their motion and thus the result of further calculations.

$$\epsilon_{photon} = \frac{1}{2}(l^2 r^{8m-2} + \dot{r}^2 r^{8m^2} - 1) \tag{73}$$

$$V_{eff_{photon}} = \frac{1}{2}(l^2 r^{8m-2} - 1) \tag{74}$$

Plotting equation 74 for several masses yields figure 6. This again shows us $m = \frac{1}{4}$ is a special case where the potential becomes a constant. For $m < \frac{1}{4}$ we obtain a potential peak at $r \to 0$ where $V_{eff} \to \infty$, while $V_{eff} \to 0$ for $r \to \infty$. For $m > \frac{1}{4}$ we find steeper and steeper increasing V_{eff} for higher masses. From here we continue in order to obtain the radial differential equation.

$$0 = -(1+2\epsilon) + l^2 r^{8m-2} + r^{8m^2}\dot{r}^2 \tag{75}$$

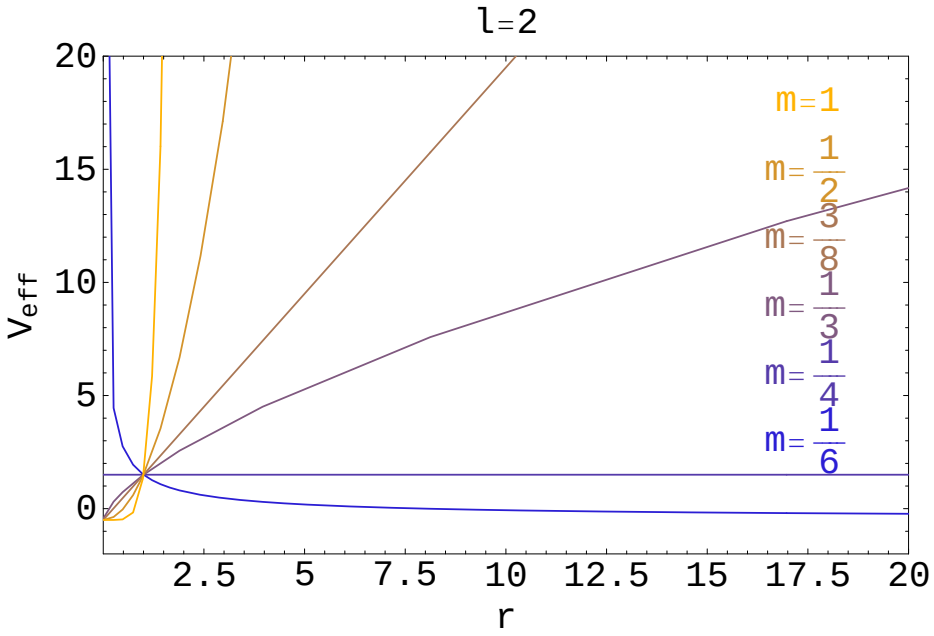

Figure 6: The effective potential: $V_{eff_{photon}} = \frac{1}{2}(l^2 r^{8m-2} - 1)$ plotted for angular momentum $l = 2$ and masses $m = \frac{1}{6}, \frac{1}{4}, \frac{1}{3}, \frac{3}{8}, \frac{1}{2}, 1$

$$0 = (4m - 1)l^2 r^{8m} + (4m^2\dot{r}^2 + r\ddot{r})r^{8m^2+2} \tag{76}$$

From equation 76 we can compute r using boundary values $r(0)$ and $\dot{r}(0)$. Plugging r back into equations 70 and 71 along with boundary values $t(0)$ and $\phi(0)$ we can compute functions t and ϕ and thus the full paths.

5.4.1 Complete motion

From the effective potential plotted in figure 6 we can predict space is very different for $m > \frac{1}{4}$ and $m < \frac{1}{4}$. To gain more insight in the specific cases and how it affects the motion of light we will take a look at $m < \frac{1}{4}$, $m > \frac{1}{4}$ and $m = \frac{1}{4}$ individually.

m = 0 First we will check the validity of our computations by taking a look at the results for empty space. The equations found by using the Weyl metric should still return the features of empty space in the absence of mass. Figure 7 shows us a set of light cones which all are perfectly uniform independent of radial distance. As we expect from flat space $\mathrm{d}t = \mathrm{d}r$. From the full radial and angular motion in figure 8 we see light travels an equal distance and along a straight path in all directions as it does in flat space.

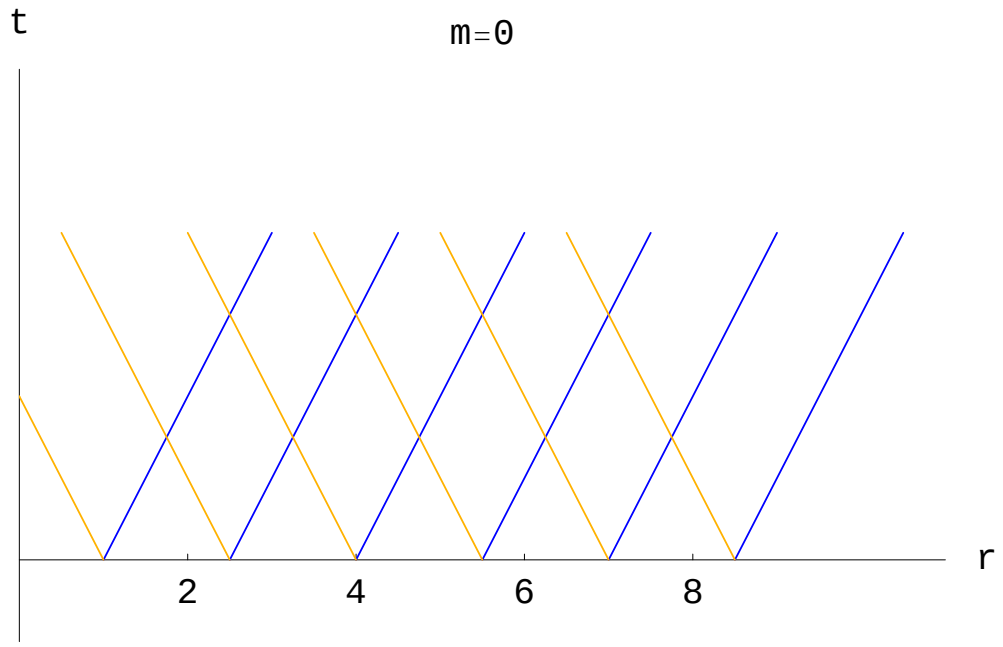

Figure 7: Light Cones with $m = 0$ plotting t as function of r with starting values $\mathrm{d}r = 1$ (blue) and $\mathrm{d}r = -1$ (orange)

$\mathbf{m < \frac{1}{4}}$ We continue onward by using a nonzero mass. As seen in figure 6 there is a multitude of special cases that need our attention. We start with $m < \frac{1}{4}$ where the potential takes the form as $Veff = \frac{1}{r}$. Figure 9 shows this effective potential for a range of angular momenta. The key feature is a singularity at $r = 0$ where $V_{eff} \to \infty$. Light can never reach $r = 0$ as was the case in the Schwarzschild metric. On the other end light is free to escape to infinity as for $r \to \infty$ $V_{eff} = -1$. Computing t and r we obtain light-cones which can be seen in figure 10. These show similar behavior as seen in the Schwarzschild metric however for a Schwarzschild radius of zero. The light-cones narrow as they approach $r = 0$ and as predicted from the effective potential light can never reach $r = 0$ while it is free to escape to $r = \infty$. Computing the full motion paths from we obtain figure 11. All light-paths end in $r = \infty$ and we can now conclude this case represents a naked singularity. An interesting feature when comparing the blue (outward bound light) in figure 11 with figure 3, describing light in the Schwarzschild metric, is that they seem much more bend in our Weyl metric compared to the Schwarzschild metric where they are almost not affected. This feature of increased bending of light will come back when we talk about deflection of light.

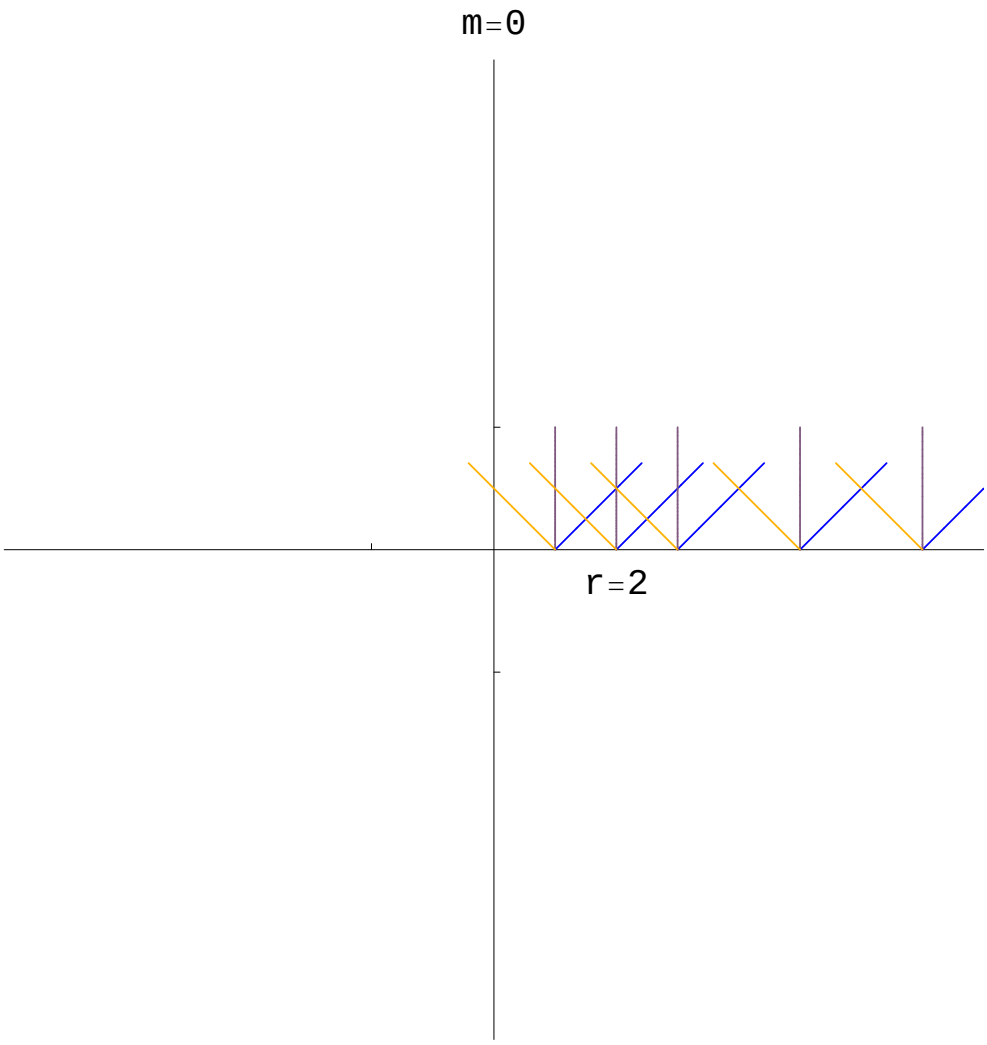

Figure 8: Graphical representation of light paths combining r and $/phi$ using starting directions $\dot{r} = 0$, $\dot{\phi} = \frac{1}{r}$ (grey); $\dot{r} = Sin(\frac{\pi}{4})$, $\dot{\phi} = \frac{Sin(\frac{\pi}{4})}{r}$ (blue) and $\dot{r} = -Sin(\frac{\pi}{4})$, $\dot{\phi} = \frac{Sin(\frac{\pi}{4})}{r}$ (orange).

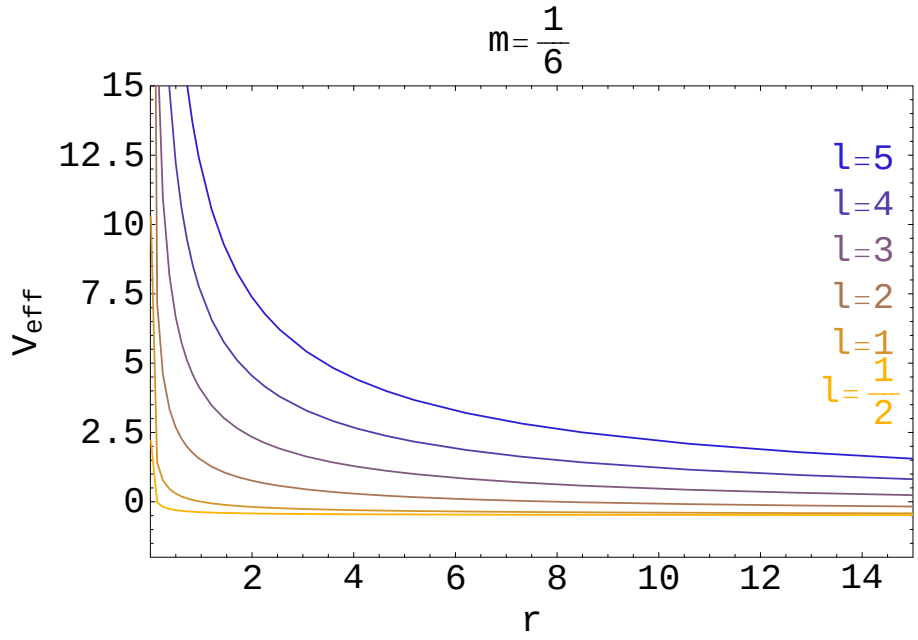

Figure 9: The effective potential: $V_{eff_{photon}} = \frac{1}{2}(l^2 r^{8m-2} - 1)$ plotted for mass $m = \frac{1}{6}$ and angular momenta $l = 5, 4, 3, 2, 1, \frac{1}{2}$

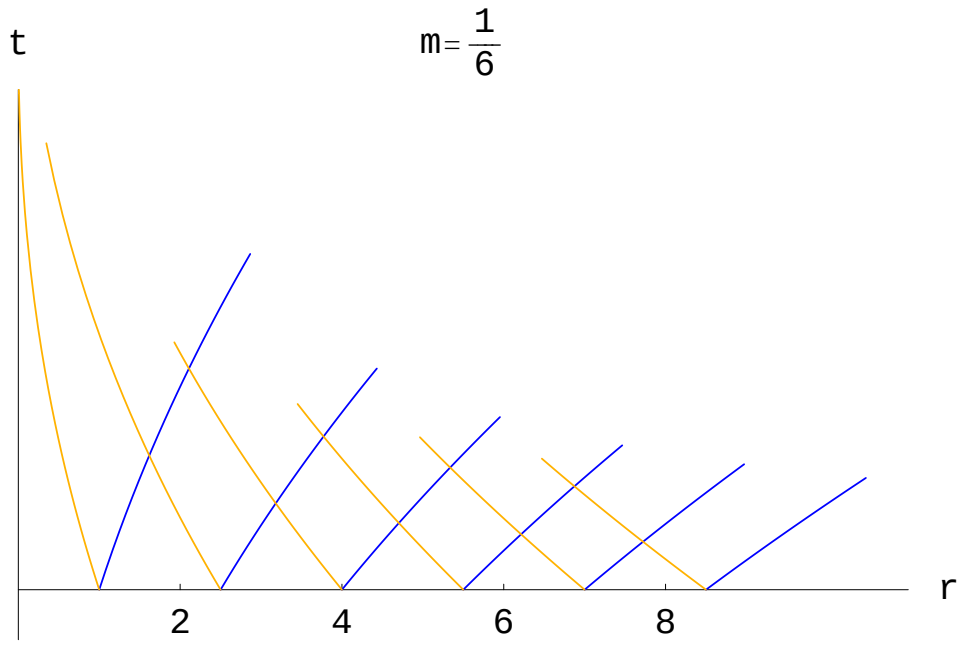

Figure 10: Light Cones plotting t as function of r with starting values $\mathrm{d}r = 1$ (blue) and $\mathrm{d}r = -1$ (orange).

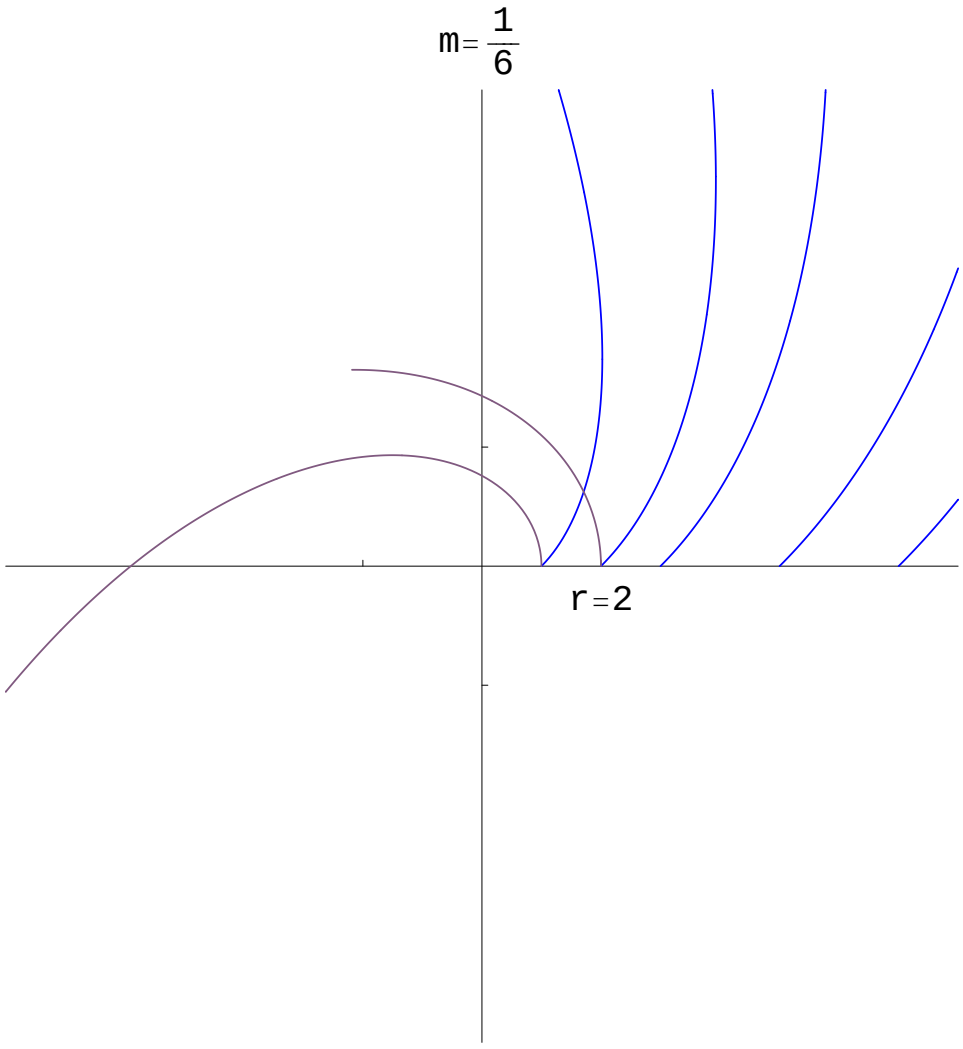

Figure 11: Graphical representation of light paths combining r and ϕ using starting directions $\dot{r} = 0$, $\dot{\phi} = \frac{1}{r}$ (grey); $\dot{r} = \sin(\frac{\pi}{4})$, $\dot{\phi} = \frac{\sin(\frac{\pi}{4})}{r}$ (blue) and $\dot{r} = -\sin(\frac{\pi}{4})$, $\dot{\phi} = \frac{\sin(\frac{\pi}{4})}{r}$ (orange).

m $> \frac{1}{4}$ We continue at the other side of the spectrum where $m > \frac{1}{4}$ and we saw in figure 6 the effective potential increased indefinitely and reached $V_{eff} = 0$ at $r = 0$. Computing V_{eff} for several angular momenta shows

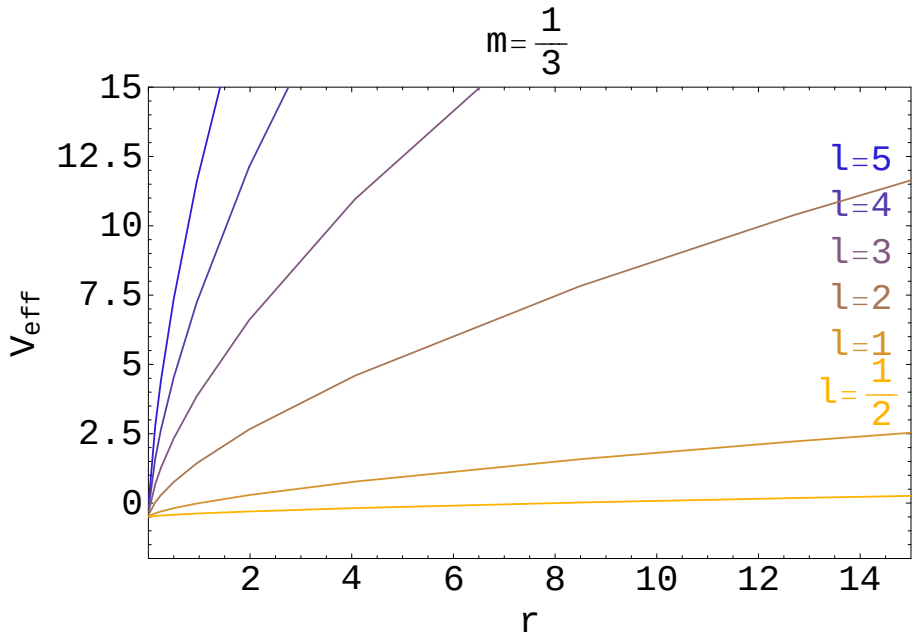

Figure 12: The effective potential: $V_{eff_{photon}} = \frac{1}{2}(l^2 r^{8m-2} - 1)$ plotted for mass $m = \frac{1}{6}$ and angular momenta $l = 5, 4, 3, 2, 1, \frac{1}{2}$.

the same features in figure 12. For this specific mass range photons will all reach $r = 0$ and can never escape to $r = \infty$. The light-cones in figure 13 obtained by computing r and t for $m > \frac{1}{4}$, contradict this statement as radially outward moving photons seem to have a positive $\dot{t}$ unlike photons moving outward inside the schwarzschild radius. Computing r and ϕ shows us that these radially outward moving photons are an exception. As seen in figure 14 all photon paths curve to $r = 0$. This situation can be described as un-physical and unsuitable for a better understanding in the bending of light.

m $= \frac{1}{4}$ The borderline case at $m = \frac{1}{4}$ finally displayed a constant V_{eff} in figure 6. A combination in the previous two cases shows light can reach $r = 0$ and escape to $r = \infty$. Computing V_{eff} for several angular momenta shows the same features in figure 15. Increasing potential as angular momentum increases however constant with r. The light-cones show great similarity with the previous two cases. However figure 16 shows us no new features. Finally the full motion paths described by r and ϕ gives us full justification

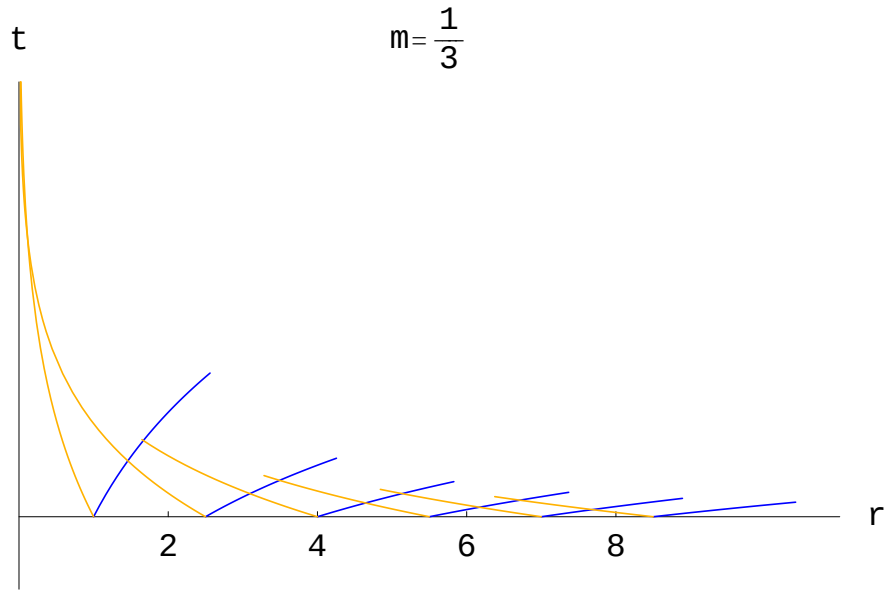

Figure 13: Light Cones plotting t as function of r with starting values $\mathrm{d}r = 1$ (blue) and $\mathrm{d}r = -1$ (orange).

to call $m = \frac{1}{4}$ a borderline case. All inward moving photons reach $r = 0$ and all outward moving photons reach $r = \infty$.

5.4.2 Deflection of light

The previous results gave sufficient insight in the behavior of light in space described by the Weyl metric to discuss deflection of light. We have shown that for $m > \frac{1}{4}$ all photons end at $r = 0$. For $m = \frac{1}{4}$ we have a similar situation only for the half of space (ie. all light directed radially towards the mass). We will therefore continue using $m < \frac{1}{4}$ to describe deflection of light. Figure 18 is the Weyl equivalent of figure 4 at mass $m = \frac{1}{6}$ where two photon paths (one passing at $r_{min} = 5$(blue) and the other passing at $r_{min} = 10$ orange) are plotted intervals or 'magnifications'. The short distance bending of light results in a large distance deflection. As seen in figure 11 the bending of light is much larger than that seen in space described the Schwarzschild metric. Light is still curved nine orders magnitude above the minimal passing distance. We notice that for $r_{min} = 5$ (blue) the light is curved a little over twice around the mass whereas for $r_{min} = 10$ (orange) curves more than twice and a half times around the mass. This behavior is also shows in figure 19 when we finally attempt to plot $\phi_{r\to\infty}$ against r_{min}. We find an ever increasing $\phi_{r\to\infty}$ for increasing r_{min}.

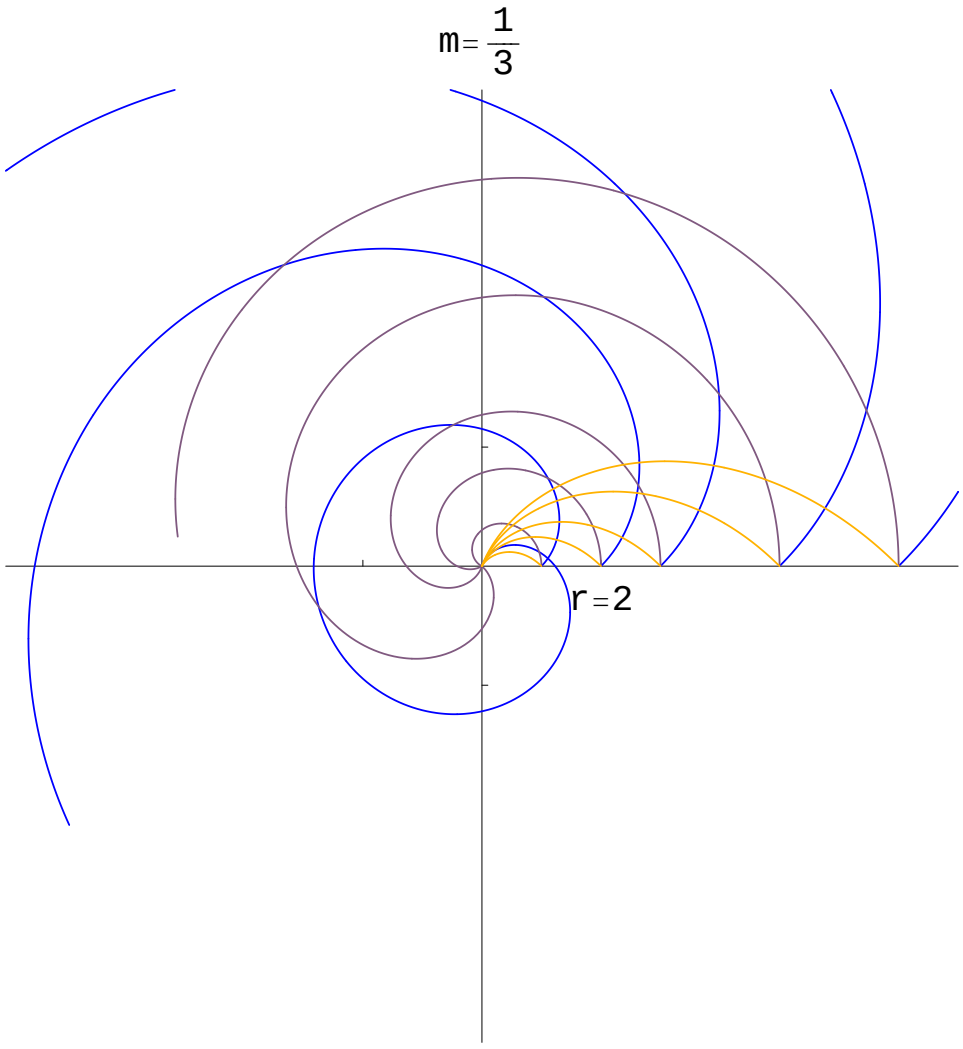

Figure 14: Graphical representation of light paths combining r and ϕ using starting directions $\dot{r} = 0, \dot{\phi} = \frac{1}{r}$ (grey); $\dot{r} = \sin(\frac{\pi}{4}), \dot{\phi} = \frac{\sin(\frac{\pi}{4})}{r}$ (blue) and $\dot{r} = -\sin(\frac{\pi}{4}), \dot{\phi} = \frac{\sin(\frac{\pi}{4})}{r}$ (orange).

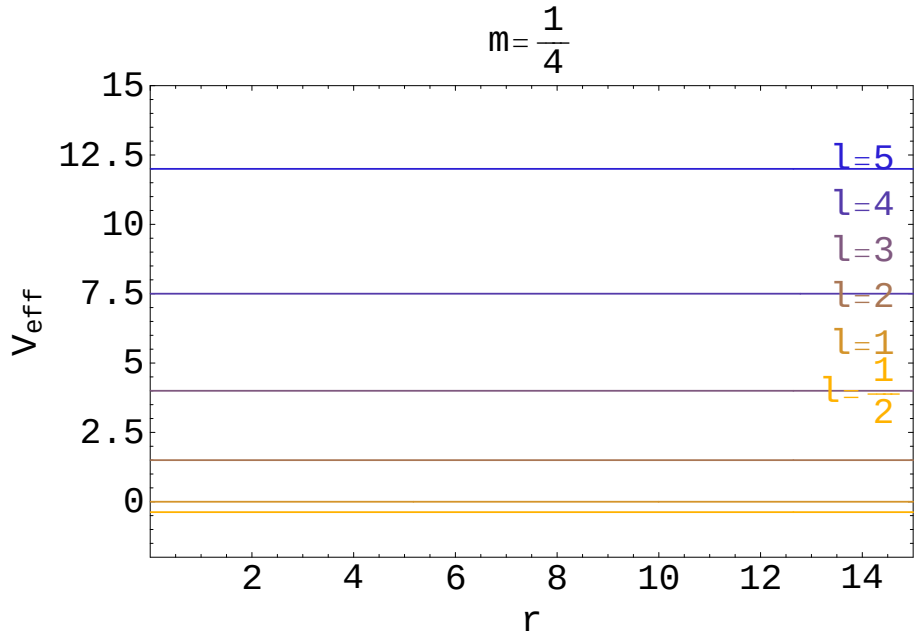

Figure 15: The effective potential: $V_{eff_{photon}} = \frac{1}{2}(l^2 r^{8m-2} - 1)$ plotted for mass $m = \frac{1}{6}$ and angular momenta $l = 5, 4, 3, 2, 1, \frac{1}{2}$

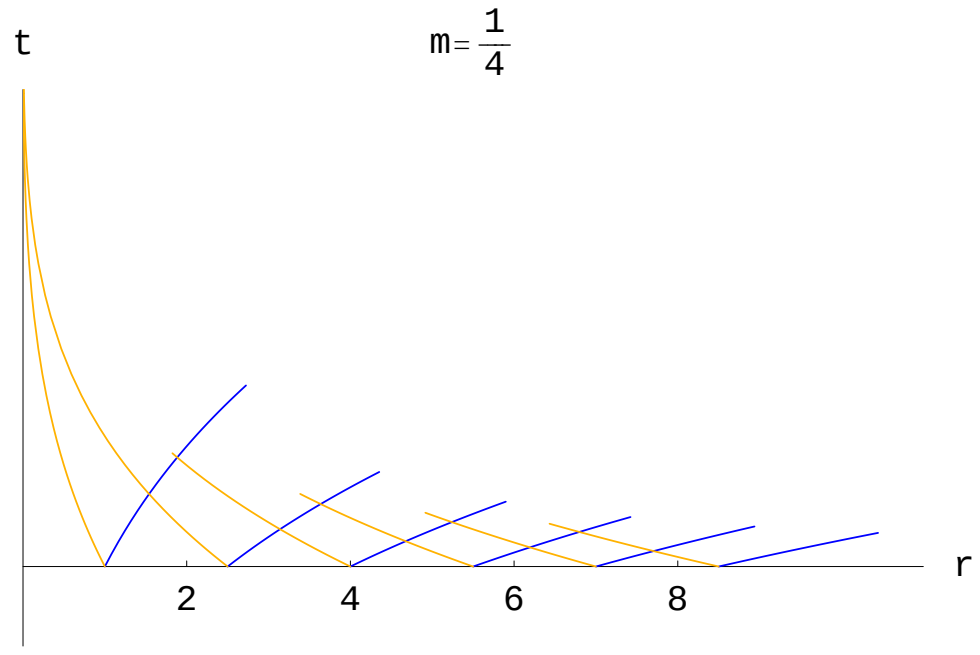

Figure 16: Light Cones plotting t as function of r with starting values $\mathrm{d}r = 1$ (blue) and $\mathrm{d}r = -1$ (orange).

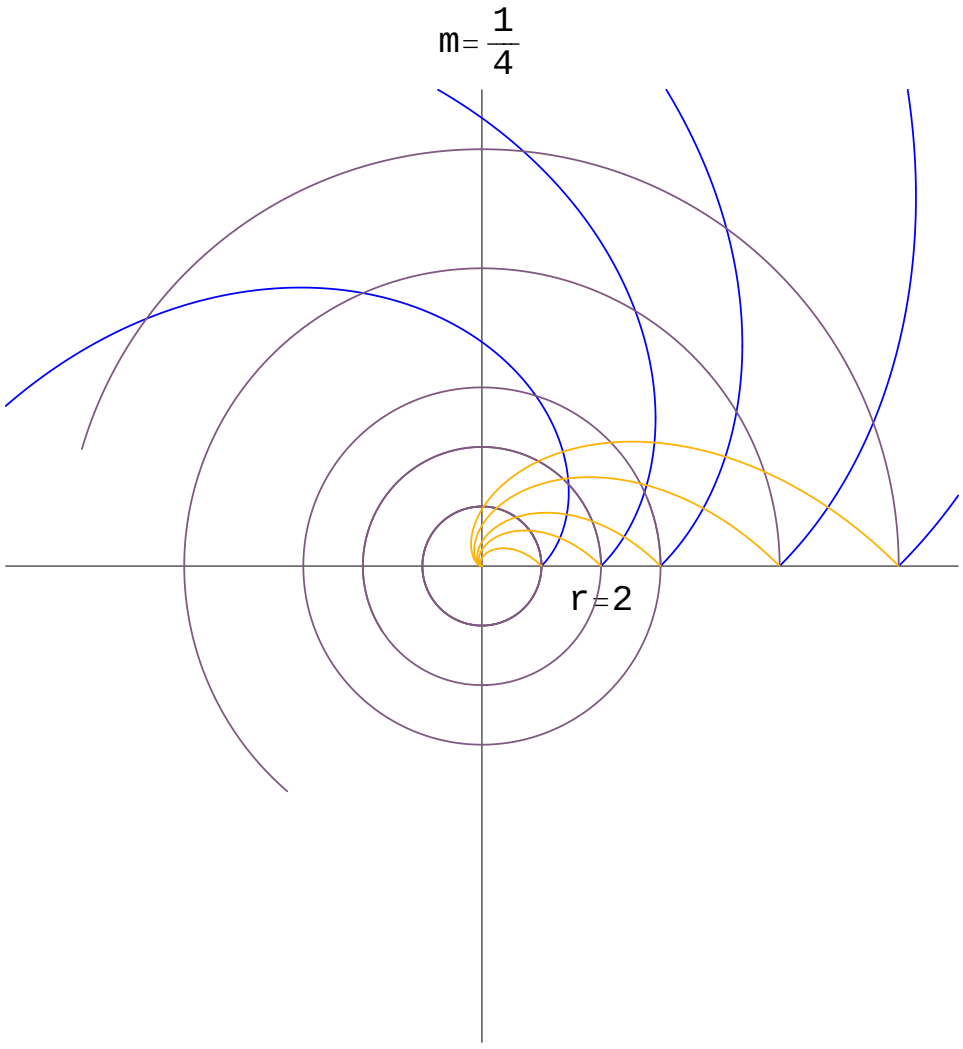

Figure 17: Graphical representation of light paths combining r and ϕ using starting directions $\dot{r} = 0$, $\dot{\phi} = \frac{1}{r}$ (grey); $\dot{r} = \sin(\frac{\pi}{4})$, $\dot{\phi} = \frac{\sin(\frac{\pi}{4})}{r}$ (blue) and $\dot{r} = -\sin(\frac{\pi}{4})$, $\dot{\phi} = \frac{\sin(\frac{\pi}{4})}{r}$ (orange).

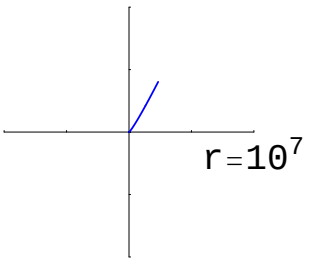

Figure 18: The path of a two single photons passing $r = 5$ (blue) and $r = 10$ (orange) at $\dot{r} = 0$ at several plot intervals.

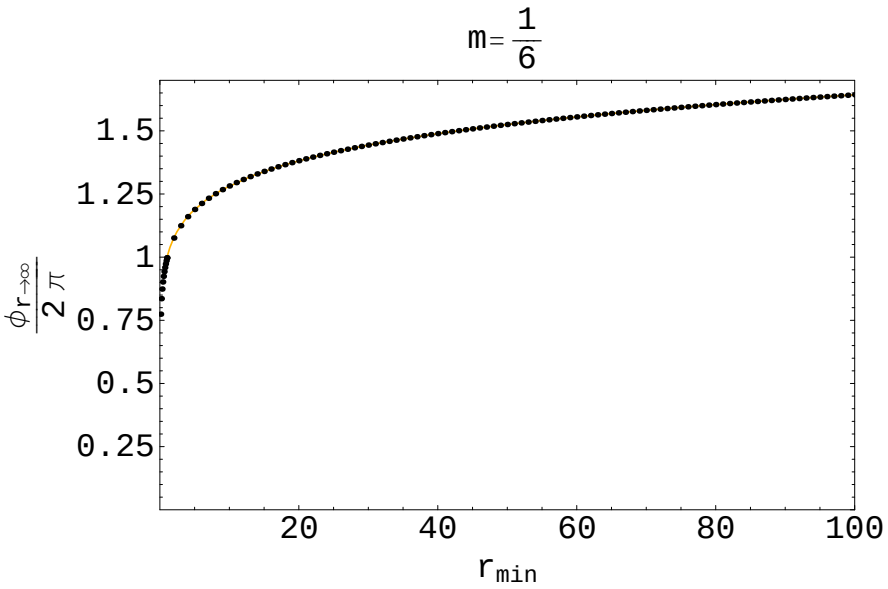

Figure 19: The deflection angle $2\phi_{r\to\infty}$ plotted against the minimal distance to the mass r_{min}. Dots: numerical calculations, Curve: fit to the data with $2\phi_{r\to\infty} = r_{min}^{a}$ where $a \approx 0.1$.

6 Another axisymmetric solution

In this section we will describe another, again simpler form, of a cylindrical symmetric metric (equation 77). We weren't able to obtain a coordinate transformation from the Weyl metric to the metric dealt with in this section.

This simple metric will, after a transformation show some of the remarkable properties of string lenses (like lensing in a flat space) that will be dealt with in the next section.

6.1 The axisymmetric metric

We start our investigation with the cylindrical symmetric metric given by

$$\mathrm{d}s^2 = -\mathrm{d}t^2 + r^{-2m}(\mathrm{d}r^2 + r^2\mathrm{d}\varphi^2) \tag{77}$$

Unfortunately, we were not able to find a coordinate transformation from the Weyl solutions to this metric. Therefore, we will first check whether this metric really is an exact solution of the Einstein field equations. Then we will apply a coordinate transformation, in order to obtain a metric which is easy to interpret geometrically.

6.2 Christoffel symbols and the Ricci-tensor

The Einstein field equations are given by the well known equation

$$G^{\mu\nu} = -\frac{8\pi G}{c^2} T^{\mu\nu} \tag{78}$$

In empty space, where $T^{\mu\nu} = 0$, it follows that $G^{\mu\nu}$ is also equal to 0. This again is equivalent to the Ricci-tensor being zero: $R_{\mu\nu} = 0$. In order to check whether this Ricci-tensor is zero, we will have to calculate all the Christoffel-symbols, in order to calculate all of its components

$$R_{\alpha\beta} = \Gamma^{\mu}_{\alpha\mu,\beta} - \Gamma^{\mu}_{\alpha\beta,\mu} - \Gamma^{\mu}_{\alpha\beta}\Gamma^{\nu}_{\mu\nu} + \Gamma^{\mu}_{\alpha\nu}\Gamma^{\nu}_{\mu\beta} \tag{79}$$

The Christoffel symbols will be calculated using the Euler-Lagrange equations $\frac{\partial L}{\partial x^\alpha} = \left(\frac{\partial L}{\partial \dot{x}^\alpha}\right)^{\cdot}$, in comparison with the geodesic equation $\ddot{x}^\alpha + \Gamma^{\alpha}_{\beta\gamma}\dot{x}^\beta\dot{x}^\gamma = 0$. The Lagrangian for this metric can be determined in the usual way ($L = g_{\alpha\beta}\dot{x}^\alpha\dot{x}^\beta$) by

$$L = -\dot{t}^2 + r^{-2m}\dot{r}^2 + r^{2-2m}\dot{\varphi}^2 \tag{80}$$

In the calculation of these Christoffel symbols, i, j will represent the spatial components (r, φ). We start with the $t-$components of the Christoffel symbols

$$\frac{\partial L}{\partial t} = \left(\frac{\partial L}{\partial \dot{t}}\right)^{\cdot} \quad \Rightarrow \quad 0 = -2\ddot{t}$$
$$\Gamma^{t}_{ij} = 0 \tag{81}$$

For the spatial components we find

$$\frac{\partial L}{\partial r} = \left(\frac{\partial L}{\partial \dot{r}}\right)^{\cdot} \quad \Rightarrow$$
$$-2mr^{-2m-1}\dot{r}^2 + (2-2m)r^{1-2m}\dot{\varphi}^2 = 2r^{-2m}\ddot{r} - 2mr^{-2m-1}\dot{r}^2 \quad \Rightarrow$$
$$\ddot{r} - (1-m)r\dot{\varphi}^2 = 0$$

So

$$\Gamma^{r}_{\varphi\varphi} = (m-1)r \tag{82}$$

and

$$\frac{\partial L}{\partial \varphi} = \left(\frac{\partial L}{\partial \dot{\varphi}}\right)^{\cdot} \quad \Rightarrow \quad 0 = (2r^{2-2m}\dot{\varphi})^{\cdot}$$
$$2r^{2-2m}\ddot{\varphi} + 2(2-2m)r^{1-2m}\dot{r}\dot{\varphi} \quad \Rightarrow \quad \ddot{\varphi} + r^{-1}\dot{r}\dot{\varphi} = 0$$

So

$$\Gamma^{\varphi}_{r\varphi} = \Gamma^{\varphi}_{\varphi r} = \frac{1}{r} \tag{83}$$

All other Christoffel symbols are zero. With these Christoffel symbols it is an easy task to calculate the Ricci-tensor. It is easy to see from its definition, that all cross-terms are zero. The only possible non-zero terms are the diagonals

$$R_{tt} = 0 \,(\text{all terms are zero.}) \tag{84}$$

$$R_{rr} = \Gamma^{\varphi}_{r\varphi,r} + (\Gamma^{\varphi}_{r\varphi})^2 = -\frac{1}{r^2} + \frac{1}{r^2} = 0 \tag{85}$$

$$R_{\varphi\varphi} = -\Gamma^{r}_{\varphi\varphi,r} - \Gamma^{r}_{\varphi\varphi}\Gamma^{\varphi}_{r\varphi} + 2\Gamma^{r}_{\varphi\varphi}\Gamma^{\varphi}_{\varphi r} = ...$$

$$... = -(1-m) - (1-m)\frac{r}{r} + 2(1-m)\frac{r}{r} = 0 \tag{86}$$

The conclusion of this is that all the Ricci-tensor components are zero and that the metric given by (77) is indeed a solution of the Einstein field equations (78).

6.3 Effective potentials

For this metric an effective potential like

$$V_{eff} = 0.5r^{2-2m}(l^2 r^{4m} - r^{2+2m}) \tag{87}$$

can be derived. For various masses and a particular (somewhat random) specific angular momentum, the effective potentials look like figure 20 on linear axes, and like figure 21 for log-log plots. If these plots are compared with the plots for the effective potential in the case of the Weyl-metric, one can see that the only differences are in the values for m, not in the shape of the lines. This difference is most likely due to the different units in which the mass is given.

If the effective potentials are the same, then the qualitative behavior of the photon orbits in this metric should be the same as well.

6.4 Conical geometry

In order to, at least qualitatively, say something about the meaning of this metric and the geometry belonging to it, we will apply a coordinate transformation given by

$$\rho = \frac{r^{1-m}}{1-m} \qquad , \qquad \theta = (1-m)\varphi \tag{88}$$

Inversion of the functions gives us

$$r = (1-m)^{\frac{1}{1-m}}\rho^{\frac{1}{1-m}} \qquad , \qquad \varphi = \frac{\theta}{1-m} \tag{89}$$

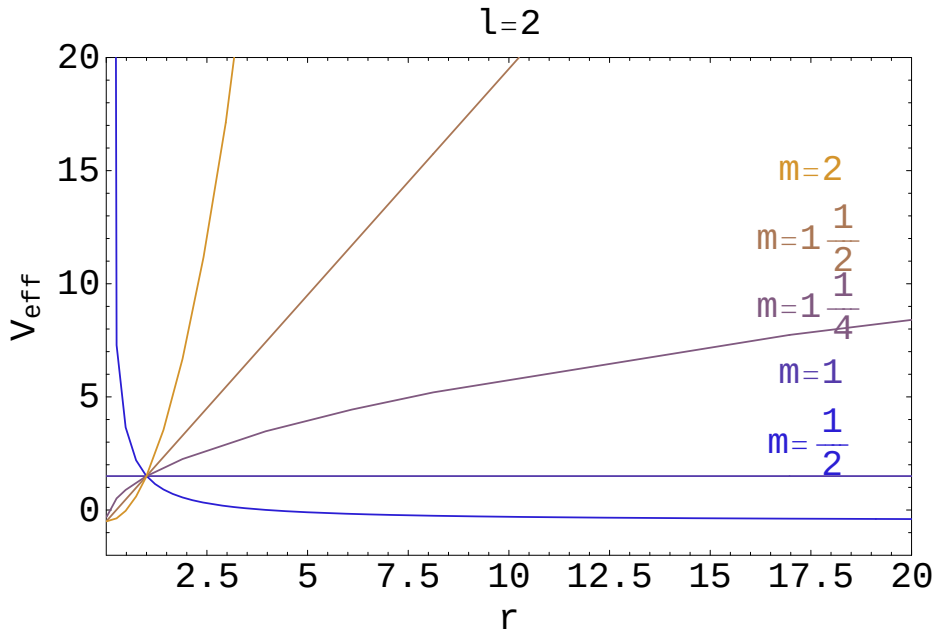

Figure 20: The effective potential for various masses, for l=2. Other values for the specific angular momentum only will give a vertical displacement of the lines.

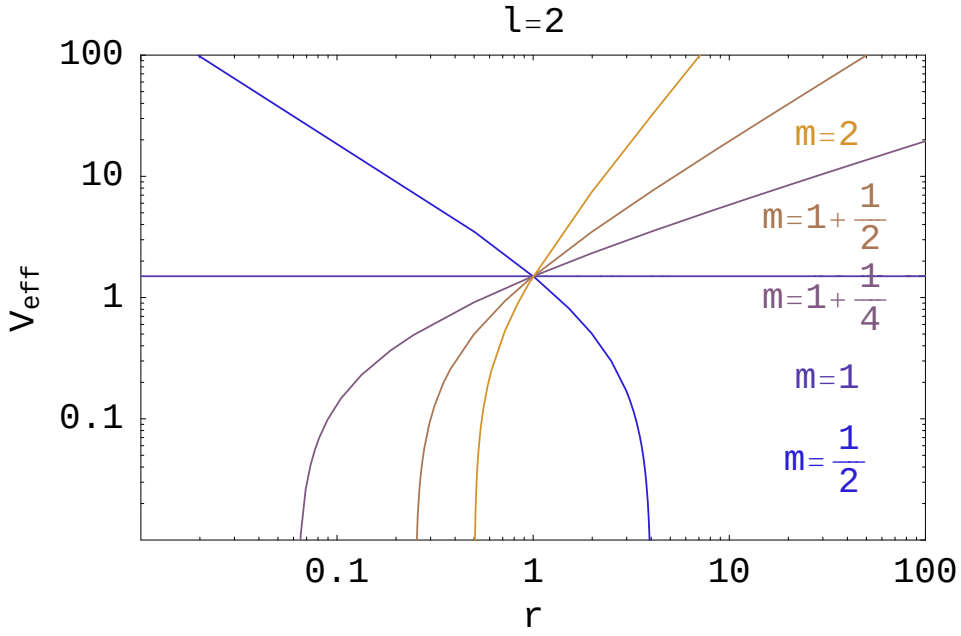

Figure 21: The same as the previous figure, now with both axes logarithmically.

and for the differentials

$$\mathrm{d}r = [(1-m)\rho]^{\frac{m}{1-m}}\,\mathrm{d}\rho \qquad , \qquad \mathrm{d}\varphi = \frac{1}{1-m}\,\mathrm{d}\theta \tag{90}$$

Mind that ρ goes from zero to infinity, as r did, but $0 \leq \theta \leq 2\pi(1-m)$, where $0 \leq \varphi \leq 2\pi$. This also puts a constraint on m: $m \leq 1$. If we apply this coordinate transformation to the metric given by (77), we obtain the following, very easy metric, which turns out to be an exact solution of the Einstein field equations as well

$$\mathrm{d}s^2 = -\mathrm{d}t^2 + \mathrm{d}\rho^2 + \rho^2\mathrm{d}\theta^2 \tag{91}$$

This of course is a very well known form of a metric: in polar coordinates this just describes a flat space! The strange thing here, however is θ, which does not run over a whole circle. This metric describes a flat space where a wedge is missing. Gluing together $\theta = 0$ and $\theta = 2\pi(1-m)$ you are left with a cone. Space-time around an infinite line mass has properties like a cone when described in these coordinates.

7 Gravitational lensing

One of the "classical" tests of general relativity is the deflection of light. In equation 91 we derived the metric of a flat space with a wedge missing. If the space is flat, how can gravitational lensing occur? Can we obtain an expression for the lens equation and/or an expression for the time delay between both images? The answers to these question will be given in this section.

In a recent paper (see [7]) fluctuations in two gravitational lensed images of a quasar (Q0957+561 A,B) were observed. The interesting thing was that the fluctuations showed no time delay in both images as would be expected when the fluctuations originated in the quasar or the lensing galaxy. The proposed solution was a cosmic string loop passing some 3 kpc from the earth. This led to the question wether or not cosmic string can produce a time delay. The answer is that it can, and the reason that it doesn't in the mentioned observation is that it's so close to Earth. In section 7.2 we will give an equation for the time delay caused by a straight cosmic string.

In another paper (see [6]) an extragalactic double source was detected. Since both galaxies look the same two possibilities were proposed. The first is chance alignment of two identical galaxies. The second is lensing by a cosmic string which produces double images without distortion.

Both probable consequences of cosmic string lensing (time delay and no distortion) will be discussed below.

7.1 Distortion-free lensing of cosmic strings

It can be shown (see [8] and our equation 91) that the geometry around a straight cosmic string is in the weak field limit locally identical to that of flat spacetime. The angular component θ does not vary between 0 and 2π but between 0 and $2\pi(1 - 4G\mu)$ (with μ being the mass per length). This is the geometry of a cone which is identical to flat spacetime with a wedge of $D = 8\pi G\mu$ removed. This wedge is called the "deficit angle" D. This configuration will produce double images in the way shown in figure 22. Since spacetime is flat, the light emitted from the quasar Q will travel

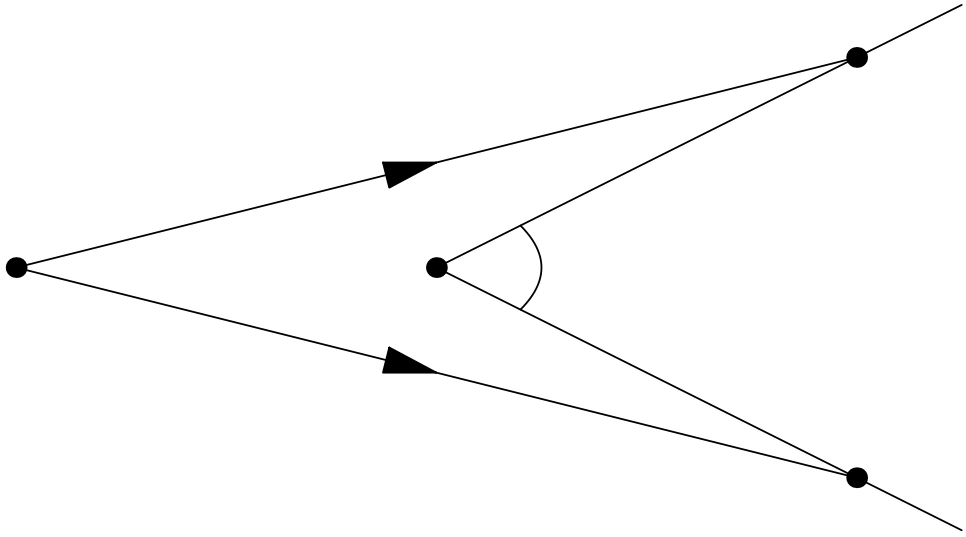

Figure 22: Conical geometry (after [8]) of a straight string. Q = quasar, S = string, D = deficit angle and O = O' = observer.

in straight lines towards the observer. The observer is both in O and in O', on both sides of the deficit angle D. The string S is located perpendicular to the plane. (If you were to "glue" the space together along the line OSO' you would get a cone.) Since the light travels in straight lines, no distortion will occur. In this particular configuration, no time delay will occur. This is not the most general case and a little more explanation is given in the next section.

7.2 Time delay in cosmic string lensing

Cosmic string lensing does not, in general, produce two images between which no time delay is observed. However it can be shown (see [2]) that a string

will produce two images (of for instance a QSO) in the sky separated by

$$\Delta\theta = D\left(\cos\alpha - \frac{1-(1+z_s)^{-1/2}}{1-(1+z_q)^{-1/2}}\right) \tag{92}$$

The first image is at an angle of θ_1 of the string and the second image is at an angle of θ_2 of the string. $\Delta\theta = \theta_1 + \theta_2$. D is the angle deficit, α is the angle between the string and the plane of the sky (which is perpendicular to the line of sight) and z_s and z_q are the redshifts for the String and the Quasar respectively.

It can also be shown (see [2]) that the time delay of a fluctuation at the QSO is given by

$$t_2 - t_1 = H_0^{-1}\left(\theta_1 - \theta_2\right) D\left[1-(1+z_s)^{-1/2}\right] \tag{93}$$

From which the no-time-delay follows as a simple consequence when $\theta_1 = \theta_2$.

8 Conclusion

In physics one always has the freedom to choose the coordinate system he or she prefers. As long as the physics can be described, you can do everything you like with your coordinates. Care has to be taken, though, that you still understand what your coordinates actually are and mean. This also became clear in the course of this report.

In order to say something useful about cosmic string lensing candidates we tried to solve the Einstein equations for an axisymmetric situation (in 3+1 dimensions, corresponding to a point mass in 2+1 dimensions). In the end we were left with two constants, one of which was determined by the Newtonian solution in the weak field limit. Because we were not able to pinpoint the other constant (using techniques that do work in the Schwarzschild metric) we switched to a (completely determined) solution found by Weyl.

In this Weyl metric, numerical methods are used to calculate photon orbits in a plane perpendicular to the direction of the extension of the line mass. In this investigation the concept of effective potential is also used. These photon orbits look very counter-intuitive, but there is qualitative agreement to what other people found.

To explain qualitatively some statements about the lensing properties of infinite line masses, yet another, very simple cylindrical symmetric metric is evaluated. After a very simple coordinate transformation, this metric (which is an exact solution of the Einstein equations as well, but we weren't able

to find an appropriate coordinate transformation from the solution of Weyl) was easily interpretable as a flat space-time with conical geometry.

In this framework we made two qualitative statements about cosmic string lensing:

1. There is no distortion of the images when they are lensed. This is so because space is flat.

2. Contrary to what observers claim in the paper about cosmic string lensing candidates, there can be a time delay between the images. This time delay is only absent if observer, string and source are exactly lined up. This is of course no different from lensing by a point mass.

This whole investigation made the simplifying approximation that the line of sight from observer to source, was perpendicular to the extension of the string. In reality this will very likely not be the case. Therefore, to calculate time delays for cosmic string lenses properly, one will have to take account of a $z-$dependence.

References

[1] A.-C. Davis and T.W.B. Kibble, *Fundamental cosmic strings*, http://arxiv.org/abs/hep-th/0505050 (2005).

[2] J. Richard Gott III, *Gravitational lensing e®ects of vacuum strings: exact solutions*, The Astrophysical Journal **288** (1985), 422–427.

[3] J. Heise, *Lecture notes on general relativity*, Utrecht University, 2005.

[4] P. Hoyng, *Relativistic astrophysics and cosmology*, Lecture Notes Astrophysics, Utrecht University, 2004.

[5] F. Quevedo, *Lectures on string and brane cosmology*, Class. Quant. Grav **19** (2002), 572–579.

[6] M. Sazhin, G. Longo, Capaccioli M., Alcalá J.M., R. Silvotti, G. Covone, O. Khovanskaya, M. Pavlov, M. Pannella, M. Radovich, and V. Testa, *CSL-1: chance projection e®ect or serendipitous discovery of a gravitational lens induced by a cosmic string?*, Mon. Not. R. Astron. Soc. **343** (2003), 353–359.

[7] R. Schild, I.S. Masnyak, B.I. Hnatyk, and V.I. Zhdanov, *Anomalous °uctuations in observations of Q0957+561 A,B: smoking gun of a cosmic string?*, http://arxiv.org/abs/astro-ph/0406434 (2004), 353–359.

[8] A. Vilenkin and E.P.S. Shellard, *Cosmic strings and other topological defects*, Cambridge monographs on mathematical physics, Cambridge University Press, 1994, ISBN 0521391539.